Chapter 5

Moving Force Identification for 1d Model

5.1 Introduction

This chapter proposes a new method to identify moving forces on a bridge. The method is a new method for identifying moving forces as they traverse a simply supported beam. The new approach is an extension of the algorithm developed by Law and Fang (2001), it applies first order Tikhonov regularisation in conjunction with dynamic programming, to predict the unknown forces from either measured displacements or strains. Both algorithms are tested using dynamic simulations from a 1d finite element model of a beam subject to moving constant and time varying forces. Further to this the moving force identification algorithm is tested using dynamic simulations from a four-degree of freedom vehicle bridge interaction model with a random road profile.

5.2 Zeroth and First Order Regularisation of Moving Forces - Theory

The application of the force identification theory outlined in chapter 2 to the problem of moving forces involves two main steps.

1. The formulation of the problem into a vector matrix differential equation suitable for dynamic programming.
2. An optimisation procedure using least squares minimisation with Tikhonov regularisation to obtain the unknown forcing functions from the transient data.

In this process the following assumptions are made about the nature of the system:

1. Changes in the stiffness, mass and damping matrices are negligible with the passage of the force.
2. The system (bridge) is at rest before the application of the load
3. The velocity of the applied loads and the axle spacing between them are known.

The first assumption on the nature of the system is justifiable for cases where the mass of the truck is small compared to the total mass of the bridge; hence the mass of the truck has little effect on the frequency of the bridge. Also the implementation of the moving force identification algorithm is based on the idea that the response of the

bridge is a function of the forces applied and not the interaction of the bridge and the truck or the nature of the road profile. The assumption is also necessary as in general in the vehicle bridge interaction problem, the mass and damping matrices of the total system (bridge and truck) change with respect to the location of the vehicle (see Gonzalez 2001) and this cannot be achieved in the inverse problem. Although the bridge may not be at rest before the passage of the force, the second assumption is a mathematical consideration that is necessary to initialize the optimization routine. Similar assumptions have been made by other authors to initialize the problem of identifying moving forces (Law et al 1997, Law & Fang 2001). It is also assumed that the velocity and axle spacing of the vehicle is known. This can be achieved through the use of additional sensors; either axle detectors on the road where pneumatic tubes are placed in the road and both velocity and axle spacing can be calculated from the recorded impulse in the tubes, or strain transducers under the bridge soffit where axles are identified from the strain record (Dunne et al 2005).

5.2.1 Formulation in Dynamic Programming Terms

The equilibrium equation of motion for a bridge subject to n_f moving forces is as follows,

$$[M_g]_{nxn}\{\ddot{y}\} + [C_g]_{nxn}\{\dot{y}\} + [K_g]_{nxn}\{y\} = [L(t)]_{nxn_f}\{g(t)\} \tag{5.1}$$

where M_g, C_g and K_g are the global mass, damping and stiffness matrices respectively and $L(t)$ is the time varying location matrix relating the n_f forces to the associated degrees of freedom in the model. Generally in finite element analysis, for a force travelling at constant velocity c, when the force is located between nodes, the force is distributed to the degrees of freedom of the model as a product of the shape functions. Herein it is assumed that the elements are sufficiently small that, whether or not the force $g(t)$ is located at a node, one can regularise as if it is.

Equation (5.1) is now converted into a vector matrix differential equation as outlined in section 2.2. The resulting equation is,

$$\left(\frac{dX}{dt}\right) = [A]\{X\} + f(t) \tag{5.2}$$

Where,

$$X = \begin{Bmatrix} y \\ \dot{y} \end{Bmatrix} \tag{5.3}$$

$$[A] = \begin{bmatrix} 0 & [I] \\ -[M_g]^{-1}[K_g] & -[M_g]^{-1}[C_g] \end{bmatrix} \tag{5.4}$$

$$f(t) = \begin{bmatrix} 0 \\ [M_g]^{-1}[L(t)] \end{bmatrix} \{g(t)\} \tag{5.5}$$

In the same way as outlined in section 2.2.1 the vector matrix differential equation is converted into a discrete time integration scheme of the form,

$$\{X\}_{j+1} = [M]\{X\}_j + [\tilde{P}]_j \{g\}_j \tag{5.6}$$

$$M = e^{[A]h} \tag{5.7}$$

where h is the time difference between the j^{th} and $j+1^{th}$ time step, and

$$[\tilde{P}] = [[M] - I][A]^{-1} \begin{bmatrix} 0 \\ [M_g]^{-1}[L(t)] \end{bmatrix} \tag{5.8}$$

In this form $[M]$ is a $2n_{dof} \times 2\ n_{dof}$ matrix representing the dynamics of the system and $[\tilde{P}]$ is a $[2n_{dof} \times n_f]$ matrix relating the forces to the model. With the above definitions, the solution to the moving force identification problem for the zeroth order regularisation can be solved in the exact same manner as outlined in chapter two.

The dynamic programming solution for the zeroth order regularisation problem begins by defining the following function:

$$f_{n-1}(X) = \min_{g_n} E_n(X_n, g) \tag{5.9}$$

Applying the principle of optimality to equation (5.9), yields a recurrence formula of the form,

$$f_{n-1}(X) = \min_{g_{n-1}}[(QX_{n-1} - d_{n-1}, W(QX_{n-1} - d_{n-1})) + (g_{n-1}, Bg_{n-1}) + f_n(MX_{n-1} + \tilde{P}_{n-1}\, g_{n-1})] \tag{5.10}$$

The derivation of the discrete matrix Riccatti recurrence equations as outlined in chapter 2 (section 2.4) is exactly the same for equation (5.10). Substituting $[\tilde{P}]$ for $[P]$ in the recurrence equations results in the modified definition for S_n defined by,

$$S_{n-1} = -2Q^T W d_{n-1} + M^T (I - H_n^T D_n \tilde{P}_n) S_n \tag{5.11}$$

5.2.2 First Order Regularisation of Moving Forces

For the first order regularisation, the forces are included in the state vector and it is the derivative of the force $\{r\}$ that is regularised. This gives a new system of equations of the form,

$$\begin{Bmatrix} X_{j+1} \\ g_{j+1} \end{Bmatrix} = \begin{bmatrix} M & \tilde{P}_j \\ 0 & I \end{bmatrix} \begin{Bmatrix} X_j \\ g_j \end{Bmatrix} + \begin{Bmatrix} 0 \\ I \end{Bmatrix} \{r\}_j \tag{5.12}$$

Equation (5.12) is rewritten as,

$$\{X\}_{j+1} = [K]_j \{X\}_j + [T]\{r\}_j \tag{5.13}$$

where, $[K]$ is a $[(2n_{dof} + n_f) \times (2n_{dof} + n_f)]$ representing the whole system, $\{X\}$ is the $\{2n_{dof} + n_f\}$ state vector containing the displacements and velocities of all nodes and the

vector of forces to be predicted, and $[T]$ is a $[(2n_{dof} + n_f) \times n_f]$ matrix. It should be noted that it is now the system matrix $[K]$ that is varying with time and $[T]$ will remain constant throughout the dynamic programming process. The dynamic programming solution for the first order regularisation of moving forces again begins by defining the function,

$$f_{n-1}(X) = \min_{r_n} E_n(X_n, r_n) \tag{5.14}$$

Again applying the principle of optimality to equation (5.14), yields a recurrence equation of the form,

$$f_{n-1}(X) = \min_{r_{n-1}}[(QX_{n-1} - d_{n-1}, W(QX_{n-1} - d_{n-1})) + (r_{n-1}, Br_{n-1}) + f_n(X_n)] \tag{5.15}$$

Substituting equation (5.13) into equation (5.15) gives,

$$\begin{aligned} f_{n-1}(X) = \min_{r_{n-1}}[&(QX_{n-1} - d_{n-1}, W(QX_{n-1} - d_{n-1})) + (r_{n-1}, Br_{n-1}) \\ &+ f_n([K]_{n-1}\{X\}_{n-1} + [T]\{r\}_{n-1})] \end{aligned} \tag{5.16}$$

As shown in Chapter 2 it can again be assumed that the recurrence formula defined in equation (5.16) can be written as a quadratic in terms of $\{X\}$. Substituting equation (2.66) into (5.16) gives,

$$\begin{aligned} &(X_{n-1}, R_{n-1}X_{n-1}) + (X_{n-1}, S_{n-1}) + q_{n-1} = \\ &\min_{r_{n-1}}[(QX_{n-1} - d_{n-1}, W(QX_{n-1} - d_{n-1}) + (r_{n-1}, Br_{n-1}) + \\ &(K_{n-1}X_{n-1} + Tr_{n-1}), R_n(K_{n-1}X_{n-1} + Tr_{n-1}) + (K_{n-1}X_{n-1} + Tr_{n-1}), S_n + q_n \end{aligned} \tag{5.17}$$

The optimal cost is found by first minimising equation (5.17) with respect to the derivative of the force $\{r\}$ to give,

$$r^*_{n-1} = [2B + 2T^T R_n T]^{-1}\{-T^T S_n - 2T^T R_n K_{n-1} X_{n-1}\} \tag{5.18}$$

where r^* denotes the optimal derivative of the force. Substituting for $[D_n]$ and $[H_n]$ as defined in equations (5.19) and (5.20) into equation (5.18) gives the optimal derivative of the force as defined in equation (5.21).

$$D_n = [2B + 2T^T R_n T]^{-1} \tag{5.19}$$

$$H_n = 2T^T R_n \tag{5.20}$$

$$r^*_{n-1} = -D_n T^T S_n - D_n H_n K_{n-1} X_{n-1} \tag{5.21}$$

Equation (5.21) is now substituted into equation (5.17) to give,

$$\begin{aligned}
&(X_{n-1}, R_{n-1} X_{n-1}) + (X_{n-1}, S_{n-1}) + q_{n-1} = \\
&(X_{n-1}, Q^T W Q X_{n-1}) - (2X_{n-1}, Q^T W d_{n-1}) + d_{n-1}, W d_{n-1} \\
&+(-D_n T^T S_n - D_n H_n K_{n-1} X_{n-1}), B(-D_n T^T S_n - D_n H_n K_{n-1} X_{n-1}) \\
&+(X_{n-1}, K^T_{n-1} R_n K_{n-1} X_{n-1}) + 2(X_{n-1}, K^T_{n-1} R_n T(-D_n T^T S_n - D_n H_n K_{n-1} X_{n-1})) \\
&+((-D_n T^T S_n - D_n H_n K_{n-1} X_{n-1}), T^T R_n(-D_n T^T S_n - D_n H_n K_{n-1} X_{n-1})) \\
&+X_{n-1}, K^T_{n-1} S_n + (-D_n T^T S_n - D_n H_n K_{n-1} X_{n-1}), T^T S_n + q_n
\end{aligned} \tag{5.22}$$

Equating like powers of $\{X\}$ with R_{n-1}, R_n, S_{n-1} and S_n gives the recurrence equations for the first order regularisation of moving forces defined by,

$$R_{n-1} = Q^T W Q + K^T_{n-1}(R_n - H^T_n D_n H_n / 2) K_{n-1} \tag{5.23}$$

$$S_{n-1} = -2Q^T W d_{n-1} + K^T_{n-1}(I - H^T_n D_n T^T) S_n \tag{5.24}$$

5.2.3 Numerical Procedure for the First Order Regularisation

The previous section outlined the theory for the first order regularisation of moving forces. For completeness, the implementation of the full numerical procedure to calculate moving forces is given here:

1. Calculate the constant parts of the system matrix for the first order regularisation, partition the first order discrete system as follows

$$K = \begin{bmatrix} K1 & K2 \\ K3 & K4 \end{bmatrix} \tag{5.25}$$

where

$$K1 = e^{Ah} \tag{5.26}$$

$$K3 = [0] \tag{5.27}$$

$$K4 = [I] \tag{5.28}$$

$$T = \begin{bmatrix} 0 \\ K4 \end{bmatrix} \tag{5.29}$$

In these equations [*K1*] is a matrix of size ($2n_{dof} \times 2n_{dof}$), [*K3*] is a matrix of zeros of size ($n_f \times 2n_{dof}$) and *K4* is the identity matrix of size ($n_f \times n_f$). It should be noted that the matrix [*K2*] is time variant, and is therefore evaluated at each time step (Step 3). This means that the total system matrix [*K*] is formulated at each time step in the forward and backward sweep of the dynamic programming routine. It would not be feasible or cost effective to construct the system matrix [K] for each time step prior to the forward and backward sweep.

2. Calculate the location matrix *L(t)* for each time step.
3. Invert the consistent mass matrix [M_g] and calculate [*K2*] for each time step as follows,

$$K2 = \tilde{P} = [K1 - I][A]^{-1} \begin{bmatrix} 0 \\ [M_g]^{-1}[L(t)] \end{bmatrix} \tag{5.30}$$

4. Initialise the discrete matrix Riccatti equations for the backward sweep, at the last time step *N* for the dynamic programming routine as follows:

$$R_N = Q^T W Q \tag{5.31}$$
$$S_N = -2Q^T W d_N \tag{5.32}$$
$$H_N = 2(T^T R_N) \tag{5.33}$$

5. Define an array of regularisation parameters λ for the calculation of the optimal regularisation parameter. For each backward sweep of the dynamic programming routine, reinitialise the B matrix of regularisation parameters as follows

$$B = \lambda \times [I] \tag{5.34}$$

Consequently reinitialise the initial condition of D_N as,

$$D_N = [2B + 2T^T R_N T]^{-1} \tag{5.35}$$

6. This is the backward sweep for a single regularisation parameter, Starting at the $j = N\text{-}1^{th}$ time step and proceeding to first time step ($j = 1$), calculate in the following order

$$R_{j-1} = Q^T W Q + K_{j-1}^T (R_j - H_j^T D_j H_j / 2) K_{j-1} \tag{5.36}$$
$$H_{j-1} = 2T^T R_{j-1} \tag{5.37}$$
$$D_{j-1} = [2B + 2T^T R_{j-1} T]^{-1} \tag{5.38}$$
$$S_{j-1} = -2Q^T W d_{j-1} + K_{j-1}^T (I - H_j^T D_j T^T) S_j \tag{5.39}$$

Note that the system matrix [*K*] is assembled at each time step from the definitions in step 1 & 3.

7. During the backward sweep, save all of the (R_j, S_j, H_j and D_j) as they are required in the forward sweep.
8. This is the forward sweep. It is assumed that the bridge is at rest before the passage of the force. This defines the initial condition for the state vector and the initial derivative of the forcing function as;

$$X_1 = 0 \tag{5.40}$$

$$r_1 = -(2B + 2(T^T R_2 T))^{-1} T^T (S_2 + 2R_2 K_1 X_1) \tag{5.41}$$

Starting at j = 2, simulate the system to the N^{th} time step using the following recurrence equations:

$$r_j = -(D_{j+1} T^T S_{j+1}) - (D_{j+1} H_{j+1}) K_j X_j \tag{5.42}$$

$$\{X\}_{j+1} = [K]_j \{X\}_j + [T]\{r\}_j \tag{5.43}$$

9. Save all of the $\{X_j\}$ and $\{r_j\}$, to calculate the error and solution norms for the L-curve defined as follows for the first order regularisation:

$$E_{norm} = (\sum_{j=1}^{N} ((QX_j - d_j), W(QX_j - d_j)))^{1/2} \tag{5.44}$$

$$F_{norm} = (\sum_{j=1}^{N} (r_j, r_j))^{1/2} \tag{5.45}$$

10. Repeat steps 5 through 9 for all of the regularisation parameters in the array λ and save the error norm and solution norm in each case. Plot the error norm versus the solution norm on log log scales and locate the optimal regularisation parameter.
11. Repeat steps 6 to 8 for the optimal regularisation parameter.

5.3 Zeroth and First Order Regularisation Results for a Single Moving Force

The zeroth and first order regularisation is applied to the scenario of a single moving load traversing the bridge model outlined in section 4.2. The method outlined in section 4.2 is used to simulate for moving a force traversing the bridge at constant velocity. In inverse dynamics there are generally measurements taken on the structure during the period of free vibration (Trujillo & Busby 1997). Therefore, in the case of a single moving force, it is assumed that the force remains at the penultimate node for a time after it has traversed the bridge, for the purposes of the inverse analysis, see figure 5.1.

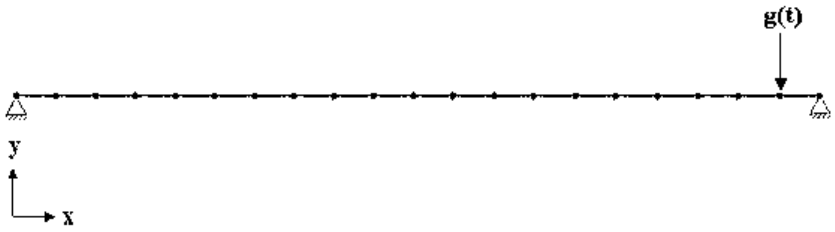

Figure 5.1 – Force remains at penultimate node for the identification of single moving forces

The bridge outlined in section 4.2 has a span of 20 m; the simulated strain at 9.5 m contaminated with 3% Gaussian noise is used as the input for the measurement vector $\{d\}$ in both the zeroth and first order regularisation. The strain is simulated at 9.5 m, as this is the middle of the 10th element in the finite element model. The [Q] matrix, which relates the measured data to the state variables, can be defined using equation (2.90). The [Q] matrix is a matrix of size (1 × 84) in the case of the zeroth order regularisation and a (1 × 85) in the case of the first order regularisation. The [Q] matrix selects the degrees of freedom of the finite element model to be compared with the measured data. The entries of the [Q] defined by equation (2.90) are defined in equation (5.46). For both cases entries 20 and 22 are equal to (-.5) and the rest are zeros

$$\varepsilon_x = \frac{-.5}{1^3}\begin{Bmatrix} 6(1)-12(.5) \\ 4(1)^2-6(1)(.5) \\ -6(1)+12(.5) \\ 2(1)^2-6(1)((.5)) \end{Bmatrix}\begin{Bmatrix} d_{19} & d_{20} & d_{21} & d_{22} \end{Bmatrix} = -.5\begin{bmatrix} 0 \\ 1 \\ 0 \\ 1 \end{bmatrix}\begin{Bmatrix} d_{19} & d_{20} & d_{21} & d_{22} \end{Bmatrix} \tag{5.46}$$

Bridge strain was simulated for a constant force of 80 kN moving at 22 m/s. Figure 5.2 a & b show the midspan strain with and without 3% noise, which is then used as the input for the inverse analysis for the zeroth and first order regularisation.

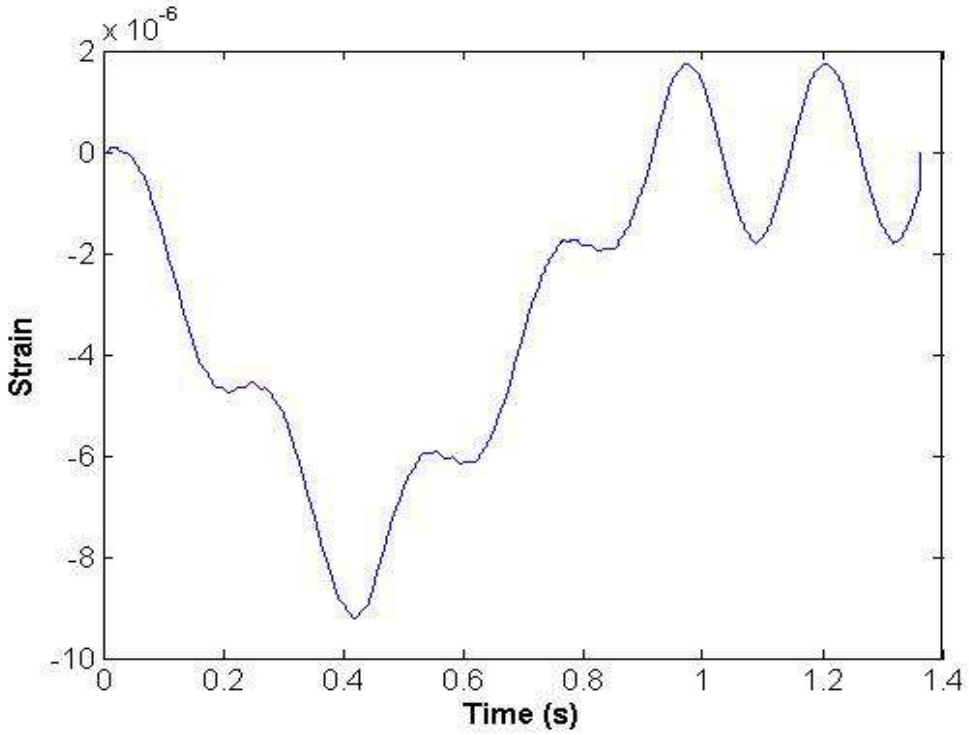

(a) - Theoretical strain

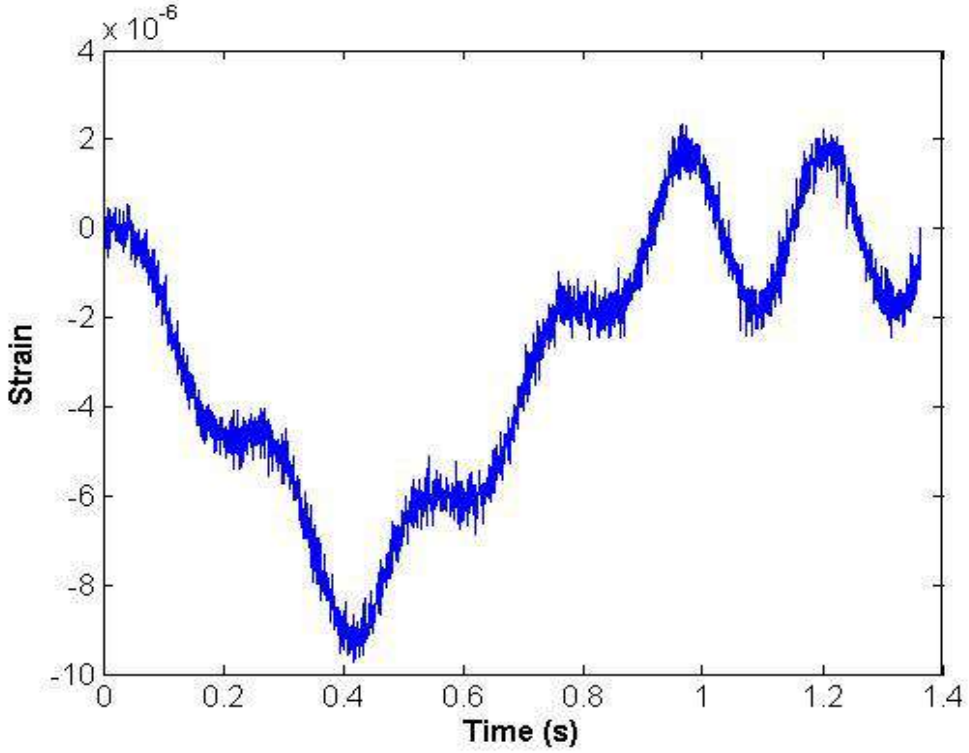

(b) – Noisy Strain

Figures 5.2 – Simulated strain at 9.5 m due to a constant load, travelling at 22 m/s

In the case of the zeroth order regularisation, the regularisation parameter λ was varied between 1×10^{-25} and 1×10^{-19}, and both the error norms and solution norms were calculated using a program developed in Matlab. In the case of the zeroth order regularisation the optimal parameter was found to lie approximately between 1×10^{-23} and 1×10^{-22} see figure 5.3. The zeroth order regularisation was then carried out and the force history calculated, for λ equal to 1×10^{-23} and 1×10^{-22} using another Matlab program. Figure 5.4 show the zeroth order regularisation for these parameters. It can be seen from these figures that the zeroth order regularisation is very sensitive to the noise added to the measurement data and the regularisation parameter itself. Figure 5.4a shows the identified force history for a regularisation parameter that is slightly closer to the least squares solution, although the trend is there, the predicted forces oscillate about the actual value of 80 kN, and when the force has traversed the bridge at approximately .9 s, the predicted forces oscillate about zero. Figure 5.4b shows the identified forces for a regularisation parameter that lies slightly to the right of the corner of the L-curve resulting in a smoother solution than that of the aforementioned parameter. Even though the solution is smoother and visible better that that using 1×10^{-23}, the results are similar to the analysis carried out on the cantilever beam. Hence it is inferred that, as in the case of the cantilever model, the first order regularisation of moving forces will provide a better solution, however this cannot be proven for all cases.

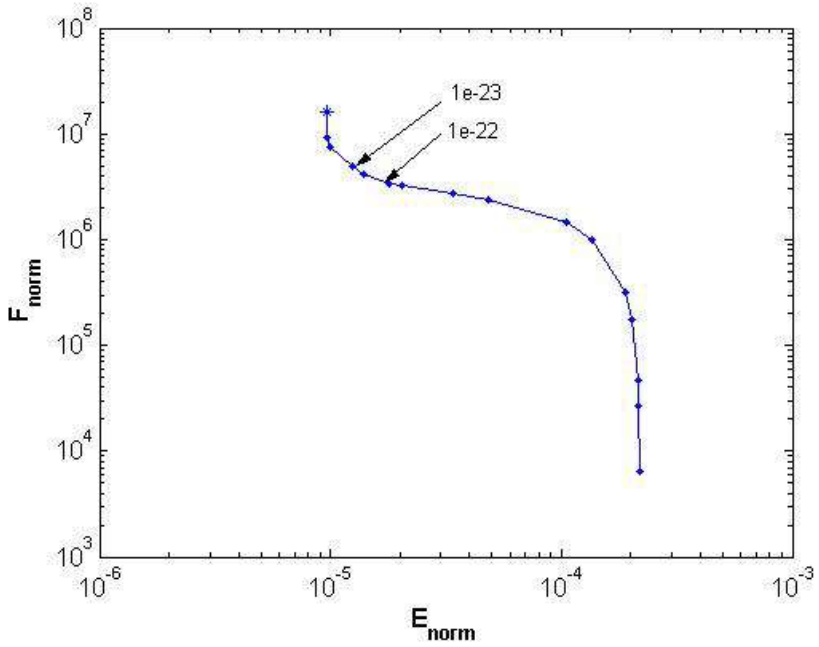

Figure 5.3 – L-curve for zeroth order regularisation of a constant load

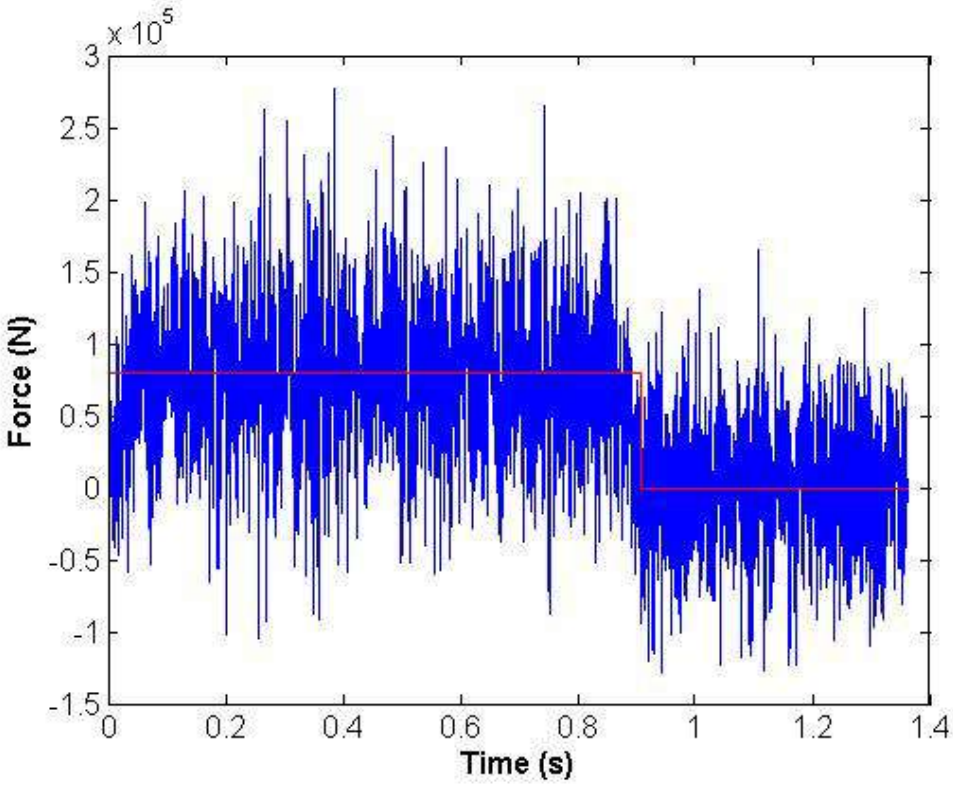

(a) - $\lambda = 1 \times 10^{-23}$, theoretical force in red, predicted force in blue

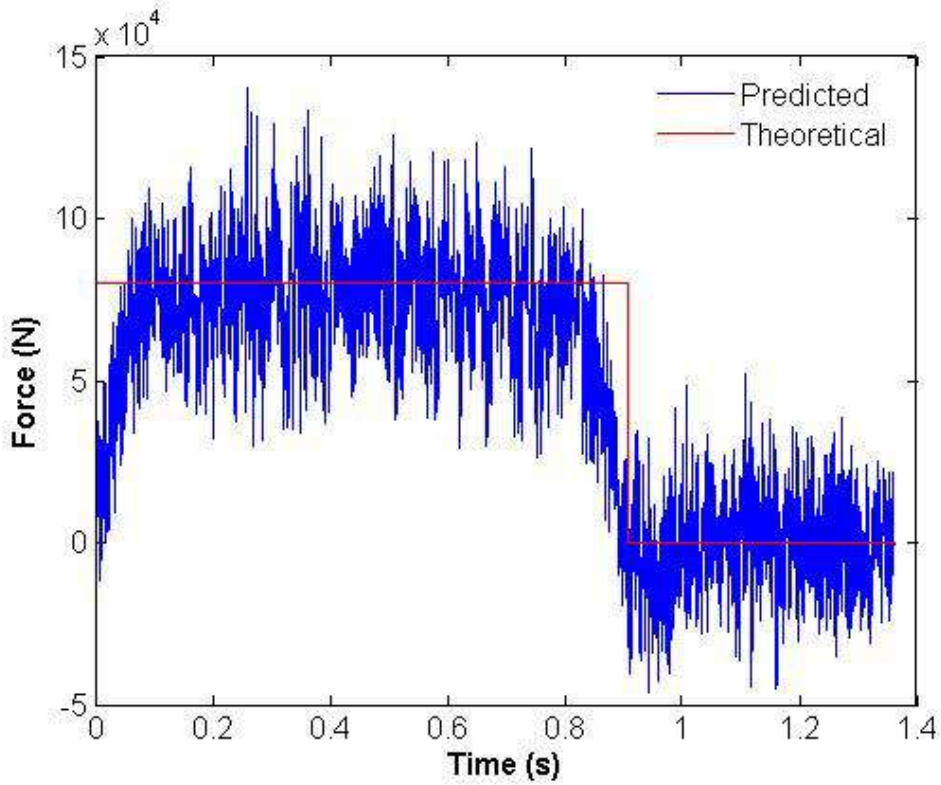

(b) –$\lambda = 1 \times 10^{-22}$, theoretical force in red, predicted force in blue

Figures 5.4 – Zeroth order regularisation of a constant load travelling at 22 m/s

In the case of the first order regularisation, the regularisation parameter λ was varied between 1×10^{-23} and 1×10^{-12}. Again both the error norms and solution norms were calculated using a program in Matlab. In the case of the first order regularisation the optimal regularisation parameter was found to lie approximately between 1×10^{-18} and 1×10^{-17}, see figure 5.5. The first order regularisation was then carried out for the λ equal to 1×10^{-18} and 1×10^{-17} using a program developed in Matlab. Figures 5.6 shows the first order regularisation for these parameters.

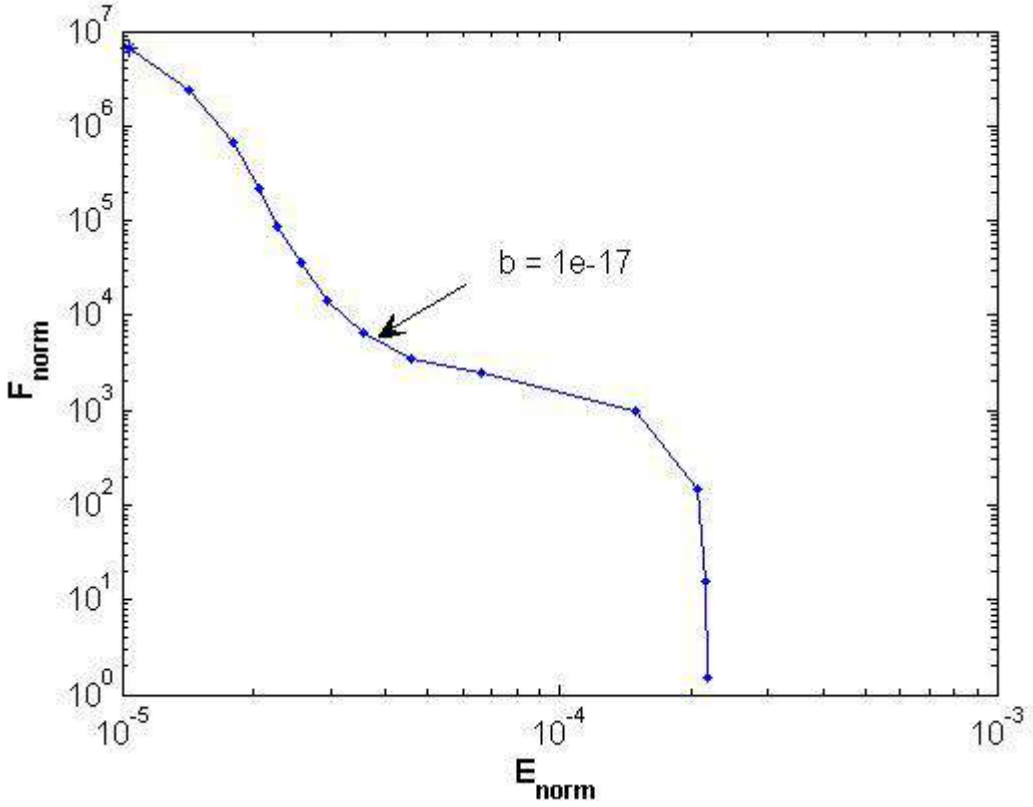

Figure 5.5 – L-curve for first order regularisation of a constant load

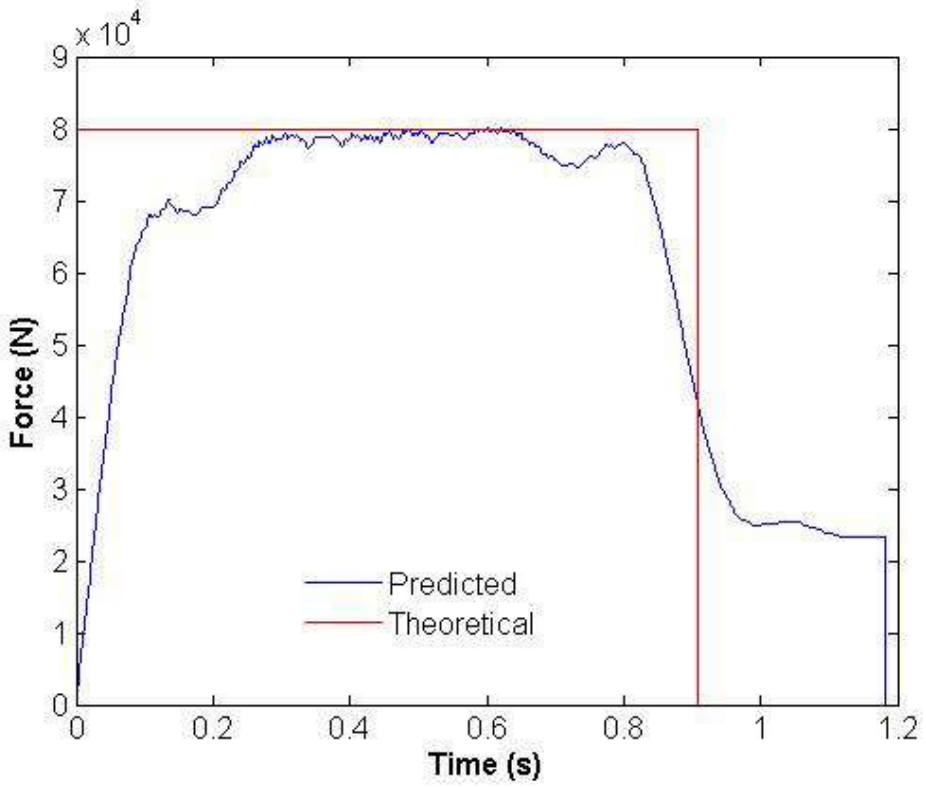

(a)- $\lambda = 1 \times 10^{-17}$, theoretical force in red, predicted force in blue

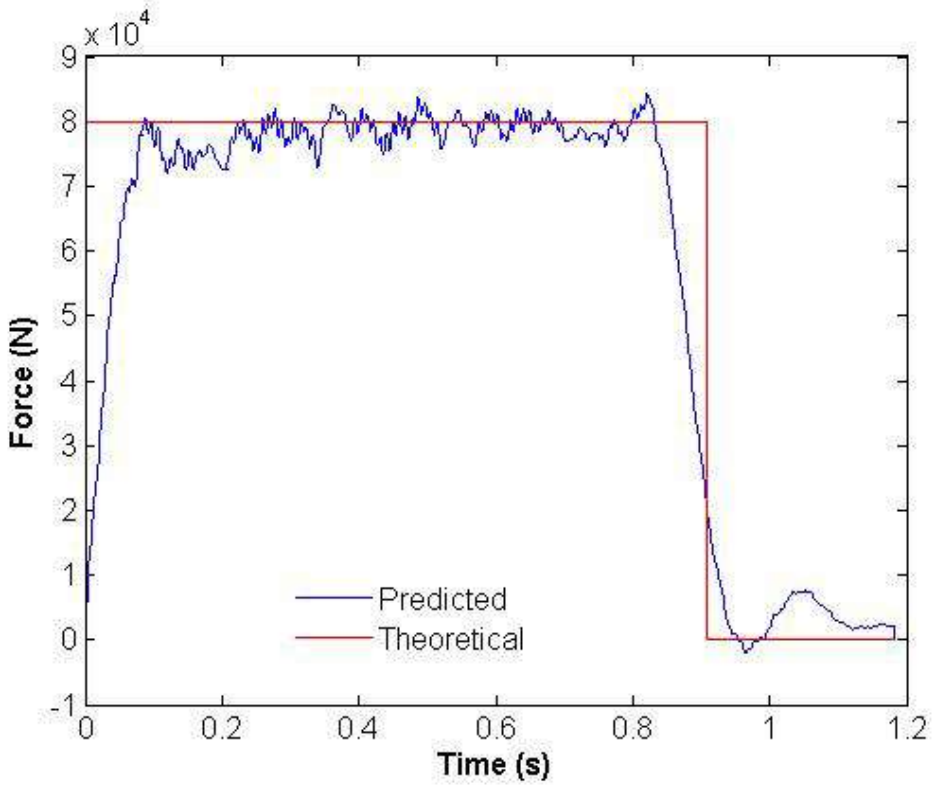

(b) - $\lambda = 1 \times 10^{-18}$, theoretical force in red, predicted force in blue

Figures 5.6 – First order regularisation of a constant load moving at 22 m/s

Figure 5.6 illustrates the effectiveness of the first order regularisation of moving loads over that of the zeroth for the case of a moving constant load. These results show the stabilising nature that is achieved by regularising for the derivative of the force as opposed to the force itself. For each of the regularisation parameters illustrated, the solutions are visible improved over that of the zeroth order regularisation. The trend of the predicted force is very similar to that of the theoretical applied force, when the force has traversed the bridge, the identified force oscillates about zero, and the error in the identified forces has been significantly improved. From this analysis alone it is assumed, however it cannot be proven that this will always be the case, that the first order regularisation provides significantly more accurate results than the zeroth order regularisation.

5.3.2 First Order Regularisation of Moving Sinusoidal Forces

Analysis was also carried out for a moving force with a sinusoidal component, to assess how the first order regularisation performs in the identification of dynamic moving loads. Two loading cases were analysed for, defined by the following functions,

(a) $$F(t) = 80000(1 + .2\sin(4\pi t)) \tag{5.47}$$

(b) $$F(t) = 80000(1 + .2(\sin(8.66)\pi t)) \tag{5.48}$$

the first loading case (a) is a simple test used to asses the accuracy of the first order regularisation under the action of a moving dynamic load. The second loading case (b) is for a force oscillating at the first natural frequency of the bridge, ie frequency matching, therefore providing a more robust test of the capabilities of the first order regularisation. Again the midspan strain was corrupted with 3% Gaussian noise. The resulting noisy signal was used as the input for the inverse analysis. The first order regularisation parameter for loading case (a) was approximately 5×10^{-18}, and 1×10^{-17} for loading case (b), and the predicted forces are shown in figures 5.7 a & b. It can be seen how, except for the time that the force is at the end portions of the bridge, the algorithm is able to predict not only the static value, but also the amplitude and the frequency of the applied force reasonably well, for both loading cases.

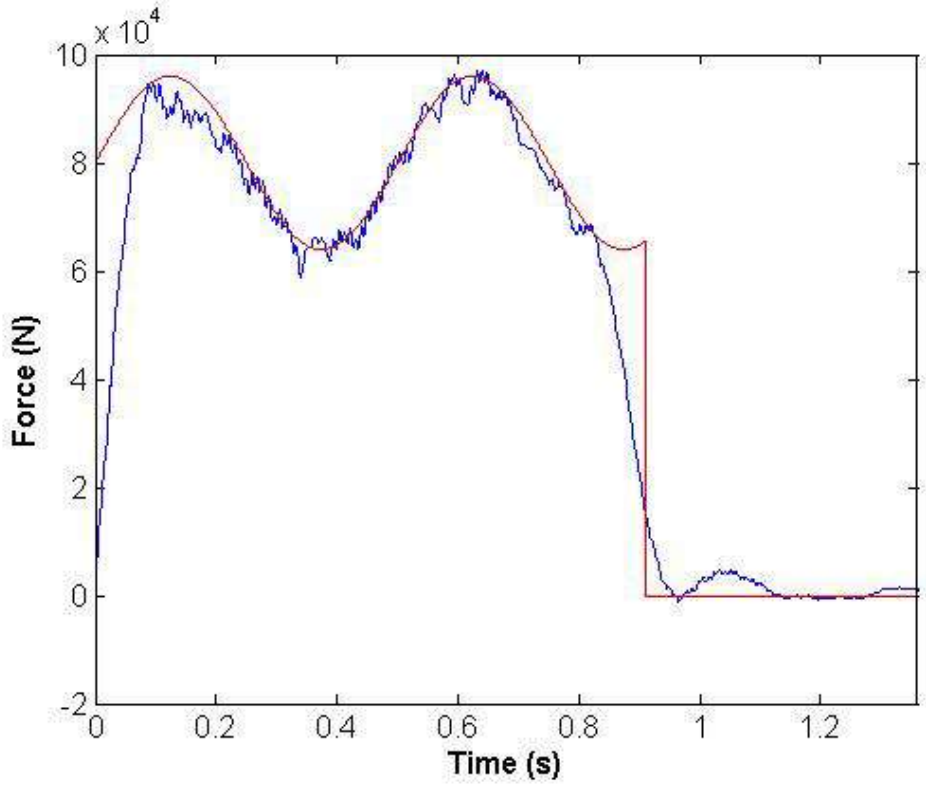

(a) – Loading case (a), $\lambda = 5 \times 10^{-18}$, theoretical force in red, predicted force in blue

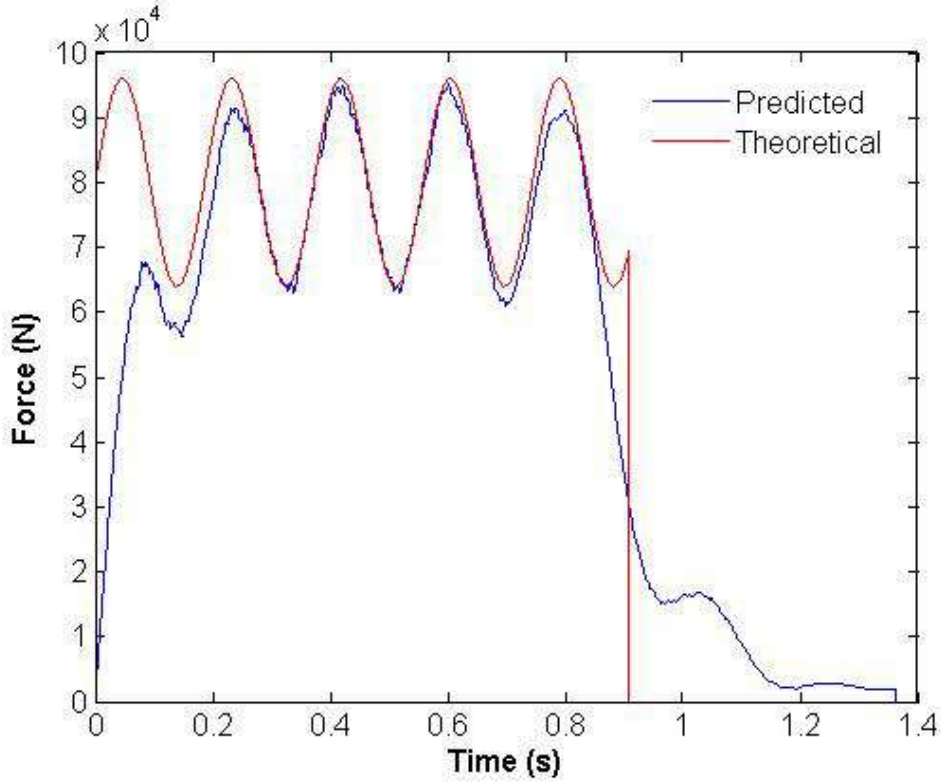

(b) - Loading case (b), $\lambda = 1 \times 10^{-17}$, theoretical force in red, predicted force in blue

Figures 5.7 – First order regularisation of a moving a sinusoidal force

5.4 First Order Regularisation of Multiple Moving Forces

In inverse dynamics there are generally measurements taken on the structure during the period of free vibration. Therefore in the case of a single moving force it is assumed that the force remains at the penultimate node for a period of time after the force has traversed the bridge for the purposes of the inverse analysis. However in the cases where there is more than one force, measurements are only taken over the time period for which there is at least one force on the bridge. This result is due to the fact that, if the same logic is extended to multiple moving forces as that of the single moving force, there would be more than one force acting on the penultimate node after the forces had traversed the bridge.

Two moving forces at a constant spacing of 5 m were simulated traversing the beam model of section 4.2. Strain was simulated at ¼, ½ and ¾ of the span length; the simulated strain corrupted with 3% Gaussian noise was then used as the input for the inverse analysis. Three different loading combinations were used to assess the accuracy of the first order regularisation of multiple moving forces. The three load combinations are,

(a)
$$\begin{aligned} F_1(t) &= 70,000 + 20,000\sin(5\pi t) \\ F_2(t) &= 100,000 + 20,000\sin(5\pi t) \end{aligned} \tag{5.49}$$

(b)
$$\begin{aligned} F_1(t) &= 70,000 + 20,000\sin(5\pi t) \\ F_2(t) &= 100,000 + 20,000\sin(5\pi t - \pi/2) \end{aligned} \tag{5.50}$$

(c)
$$\begin{aligned} F_1(t) &= 70,000 + 20,000\sin(5\pi t) + 500\sin(30\pi t) \\ F_2(t) &= 100,000 + 20,000\sin(5\pi t - \pi/2) + 500\sin(30\pi t) \end{aligned} \tag{5.51}$$

The three loading combination are chosen to approximately represent some of the dynamic components that would be present on a fully loaded 2 axle rigid vehicle, but more so to assess the accuracy of the first order regularisation. The loading combination (a) is a simple check to confirm that the first order regularisation can identify moving dynamic forces which have the same dynamic component in phase but with a different static value. The second load combination (b) is similar to (a) but there is a phase shift between the dynamic components of the force, to assess whether a phase angle between

the applied forces affects the accuracy of the first order regularisation. The third load combination (c) contains a higher frequency dynamic component corresponding to 15Hz, to check if the higher frequency affects the identified results, and if the first order regularisation can identify this frequency.

Figure 5.8 shows the first order regularisation of load combination (a) using two 'measurements' at quarter and midspan of the bridge. It can be seen from this figure that for the time periods when there is only one force on the bridge, the first order regularisation can reasonably predict the applied forces. However over the time period when there are two forces on the bridge, the first order regularisation cannot distinguish between the two forces, hence an average between the two loads is identified during this period. From this case it was found that the number of measurements required need to be greater than the number of forces present, see figure 5.9. Figure 5.9 shows, that by increasing the number of measurements from 2 to 3, results in a reasonably accurate identification of the moving forces over the period when both forces are present on the bridge.

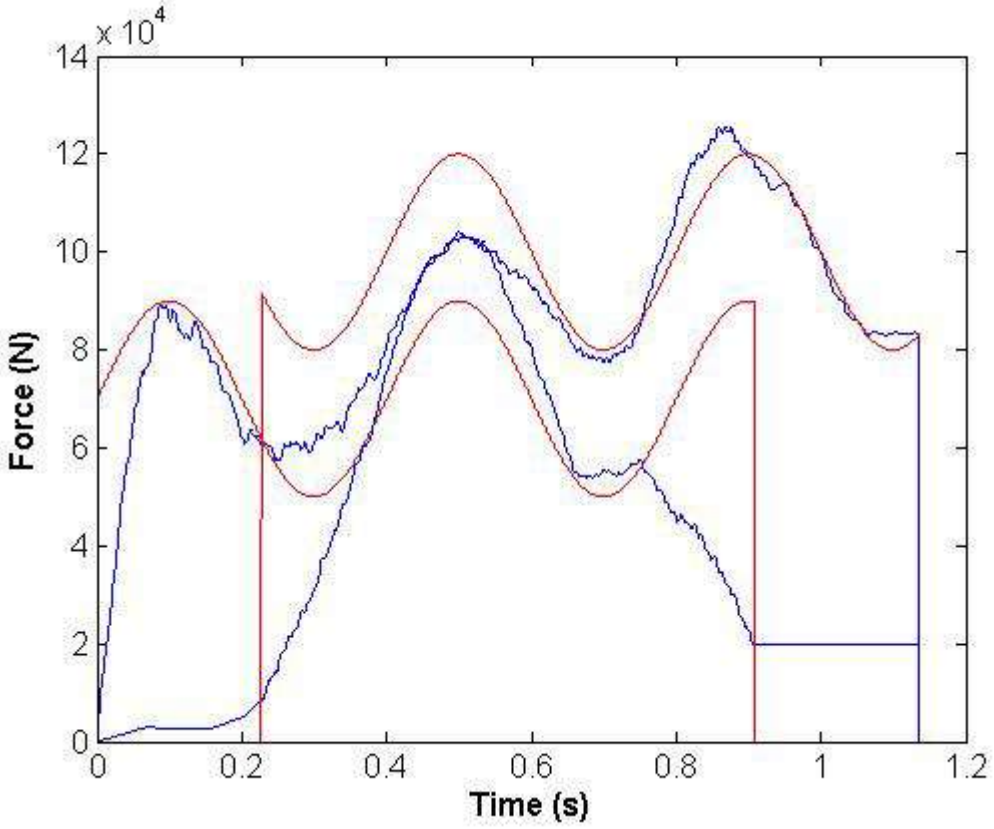

Figure 5.8 – First order regularisation for load combination (a) using 2 measurements, at ¼ and mid span, $\lambda = 5 \times 10^{-18}$, theoretical force in red, predicted force in blue

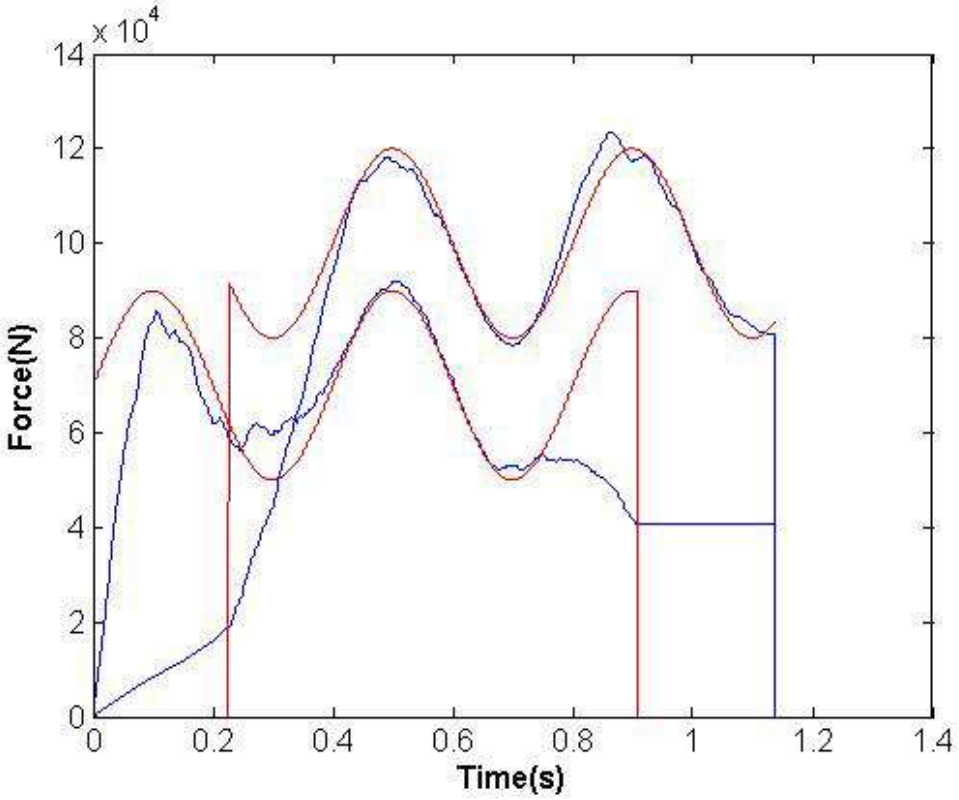

Figure 5.9 – First order regularisation for load combination (a), using 3 measurements, $\lambda = 1 \times 10^{-17}$, theoretical force in red, predicted force in blue

Figures 5.10 and 5.11, show predicted (blue) versus actual forces (red) for load combinations (b) and (c). The regularisation parameters λ were found from the L-curve as 1×10^{-17} and 1×10^{-18} respectively. Figures 5.10 and 5.11 illustrate the effectiveness of the first order identification of moving forces. The algorithm is able to accurately predict moving forces in or out of phase, and more importantly, in loading case (c) the first order regularisation is able to capture the higher frequency which is acting at 15 Hz.

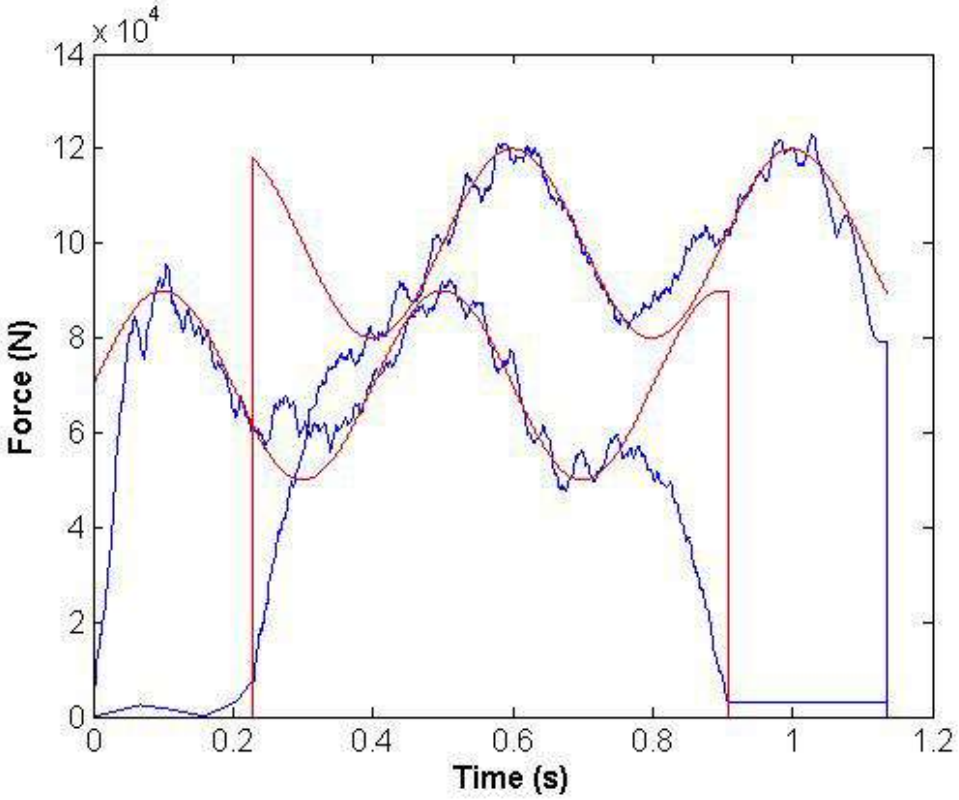

Figure 5.10 – First order regularisation for load combination (b), using 3 measurements, $\lambda = 1 \times 10^{-17}$, theoretical force in red, predicted force in blue

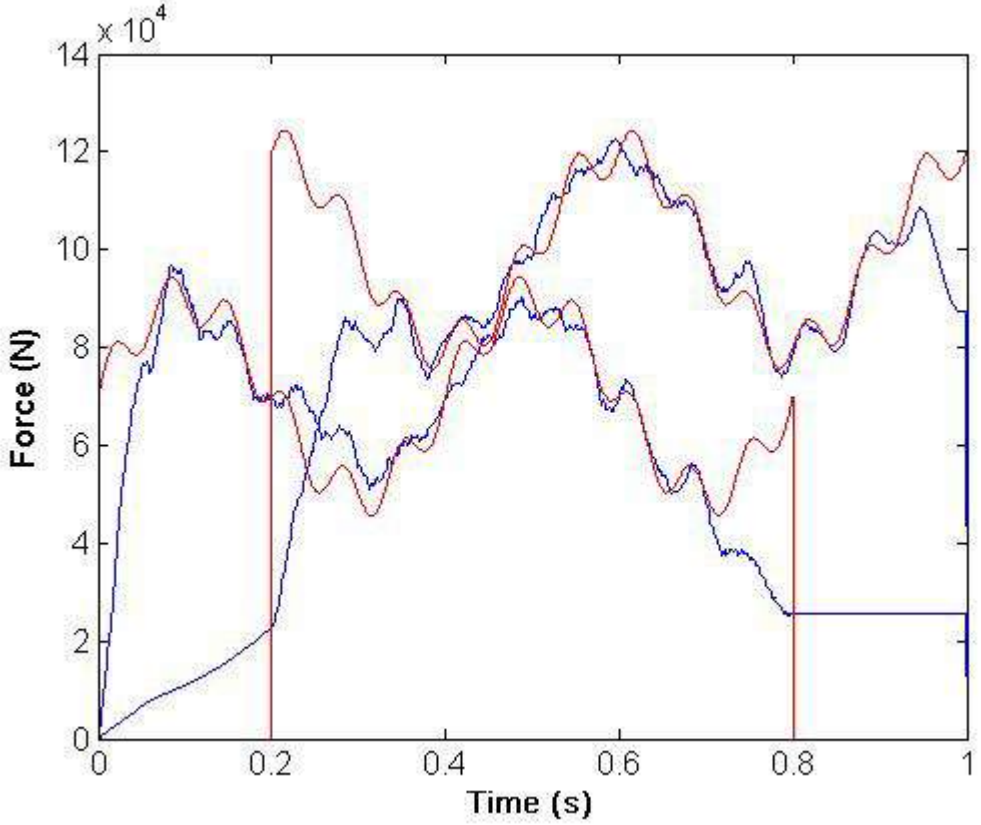

Figure 5.11 – First order regularisation for load combination (c), using 3 measurements, $\lambda = 1 \times 10^{-17}$, theoretical force in red, predicted force in blue

5.5 Prediction of moving sprung masses

The dynamic simulation outlined in section 4.2 does not account for the interaction between the truck suspension system and the bridge, nor does it take into account the effect of the road profile interaction. In order to assess the accuracy of the moving force identification algorithm outlined in section 5.4, it is necessary to carry out simulations for a vehicle bridge interaction model. Using the resulting simulated strain as an input into the moving force identification algorithm, the accuracy of the algorithm for calculating the interaction force can be assessed.

5.5.1 Vehicle Bridge Interaction Model

The bridge response due to a planar two-axle body is implemented with the numerical methods proposed by Frýba (1971) and implemented in a program developed by Gonzalez (2001). Figure 4.35 shows the four degrees of freedom of the model, allowing for pitch and bounce of the truck body. The vehicle parameters are: speed (c), axle spacing (D), body inertia (J), sprung mass ($m_s=m_{s1}+m_{s2}$), unsprung masses (m_{u1} and m_{u2}), tyre stiffness (K_{ti}), and suspension damping (C_i) and (K_{si}) suspension stiffness at each axle.

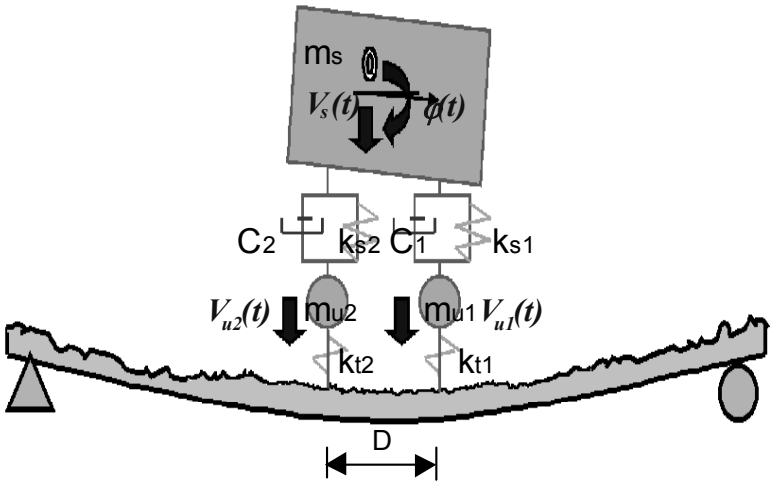

Figure 5.12 – Numerical Simulation (Fryba model)

The four degree of freedom vehicle bridge interaction model also allows for the effect of road irregularities. The height of the road irregularities r are generated from the formula

$$r(t) = \sum_{i=1}^{T} \sqrt{4S(\omega_i)}\Delta\omega \cos(\omega_i t - \theta_i) \tag{5.52}$$

Where $S(\omega_i)$, ω_i, θ_i and T are the, power spectral density function, circular frequency, uniformly distributed random variable in the range 0 to 2π and the number of discrete frequencies respectively. The road roughness is classified using the ISO (**I**nternational **S**tandards **O**rganisation) specifications; the power spectral density function for highway road roughness is defined by,

$$\begin{aligned} \omega \le \frac{1}{2\pi} cycle/m \Rightarrow S(\omega) = \frac{a}{(2\pi\omega)^2} \\ \omega > \frac{1}{2\pi} cycle/m \Rightarrow S(\omega) = \frac{a}{(2\pi\omega)^{1.5}} \end{aligned} \tag{5.53}$$

where a is the roughness co-efficient defining the quality of the road ranging from very good to very poor. The bridge properties outlined in section 4.2 have again been adopted for this study, and the vehicle parameters are speed ($c = 15, 20$ or 25 m/s), axle spacing ($D = 5$m), body inertia ($J = 1.2 \times 10^3$ kgm^2), sprung mass ($m_s = m_{s1} + m_{s2}$) where the total sprung mass is dependent on the loading condition and the sprung mass of each axle (m_{s1}, m_{s2}) is dependent of the centre of gravity for the particular loading condition. The unsprung masses (m_{u1} (*1000* kg) and m_{u2} (*1000* kg)), and at each axle, tyre stiffness ($K_{ti} = 3.6$ x 10^6 N/m), damping (C_i = 4000 Ns/m) and suspension stiffness ($K_{si} = 1.8 \times 10^6$ N/m). In order to test the accuracy for the predicted forces, a total of 18 different runs were carried out: three levels of speed (15, 20 and 25 m/s), three levels of loading (empty (2000 kg), half-full (8000 kg) and fully laden (14000 kg)) and two random road profiles (a = 8×10^{-6} ' very good', $a = 128 \times 10^{-6}$ 'poor').

The forward solution has been generated using a Runge-Kutta formulation implemented by Gonzalez (2001), as described by Frýba (1971). The generated theoretical strain is contaminated with Gaussian noise as defined in equation (4.29) (3% of the maximum strain) to simulate more realistic 'measurements'. The simulated measurements are taken at five locations (4, 8, 10, 12 and 16 metres) along the span of 20m, that are used as input for calculating the unknown applied interaction forces $\{f(t)\}$ for each axle. In the inverse analysis the number of elements in the beam model is increased from 20 to 40 giving 82 degrees of freedom, and the sampling time is reduced to 0.001 s.

5.5.2 Results on a good profile

The profile is generated from power spectral density functions for a 'good' road profile as suggested by ISO standards, a random profile is generated for each particular run. For an empty vehicle (2000 kg) moving at 25 m/s the theoretical strain measurements are generated, and then contaminated with 3% Gaussian noise see figures 5.13. The optimal regularisation parameter λ is obtained from the L-curve as approximatel $\lambda = 1 \times 10^{-18}$ see figure 5.14. Figure 5.15 shows the predicted applied forces as inferred by the first order regularisation. Vehicle dynamics for the good profile are generally quite small so the moving force can be viewed as constant forces for the lightly loaded truck. The results of the first order regularisation of the moving interaction forces are similar to the analysis carried out on the regulaisation of a moving constant force in section 5.3.1. In both cases the identified forces are quite noise, the identified interaction forces tend to oscillate about the static value of the force. The errors in identified interaction forces are most significant at the entry and exit of the second and first axles of the truck, figure 5.15 shows that, when the second axle enters the bridge there is an impulse response in the identified forces of the first axle, and conversely at the exit of the first axle there is corresponding impulse response in the identified forces of the second axle. In general the identified interaction forces for an empty vehicle travelling at 25m/s on a good profile are typical of the results found in the other case. Figures 5.16 and 5.17 represent typical identified axle forces for the results on a smooth profile.

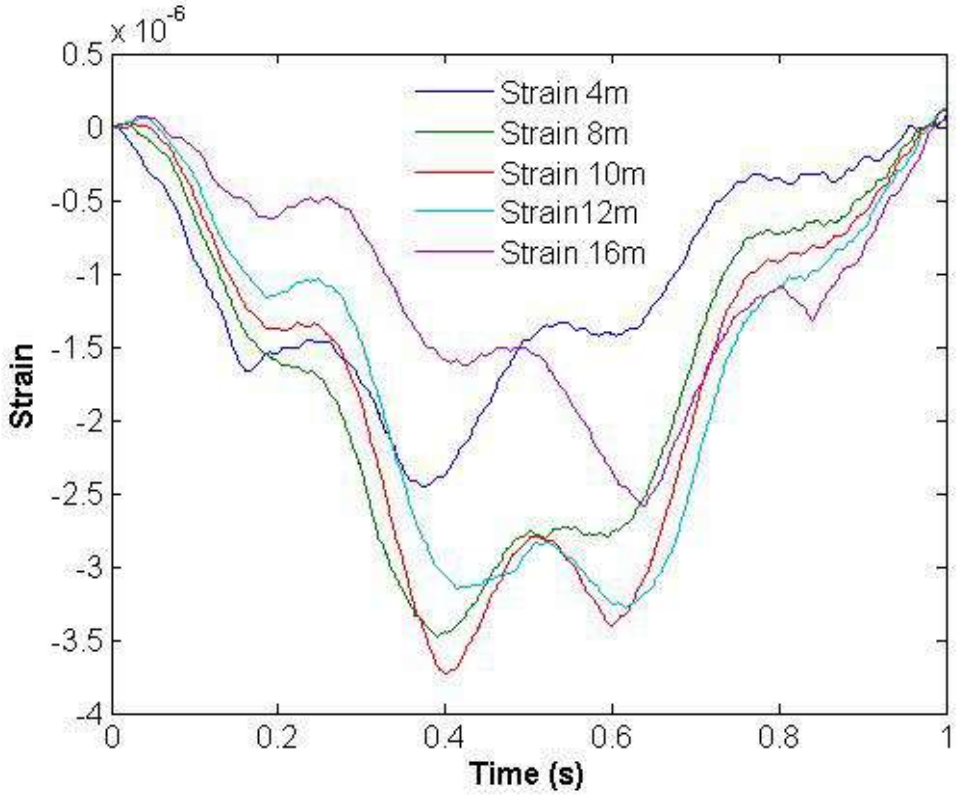

(a) – Theoretical strains

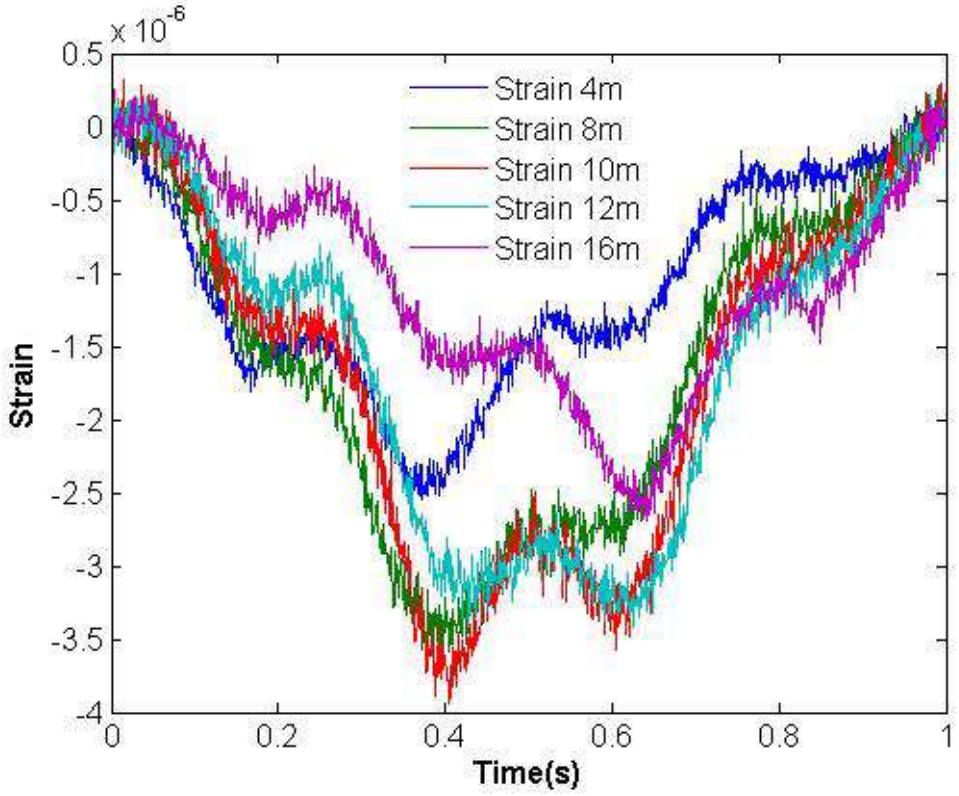

(b) – Noisy Strains

Figures 5.13 –Strain due to an empty vehicle traveling at 25m/s on a good road profile profile

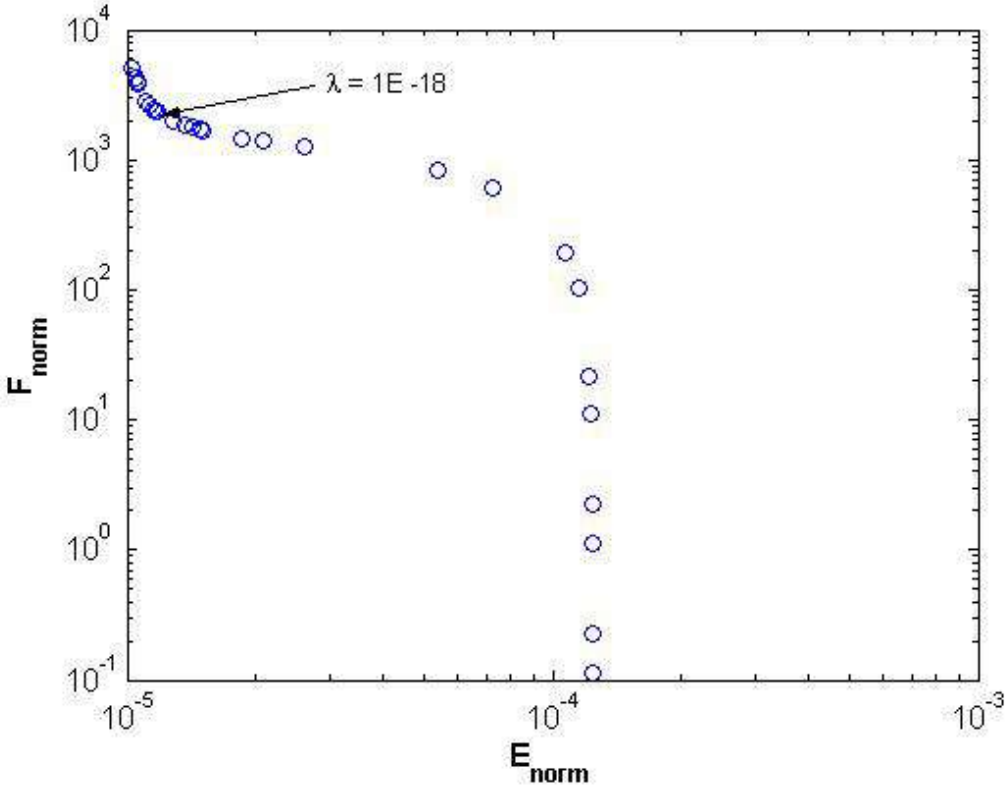

Figure 5.14 – L curve for an empty vehicle travelling at 25m/s on a good profile

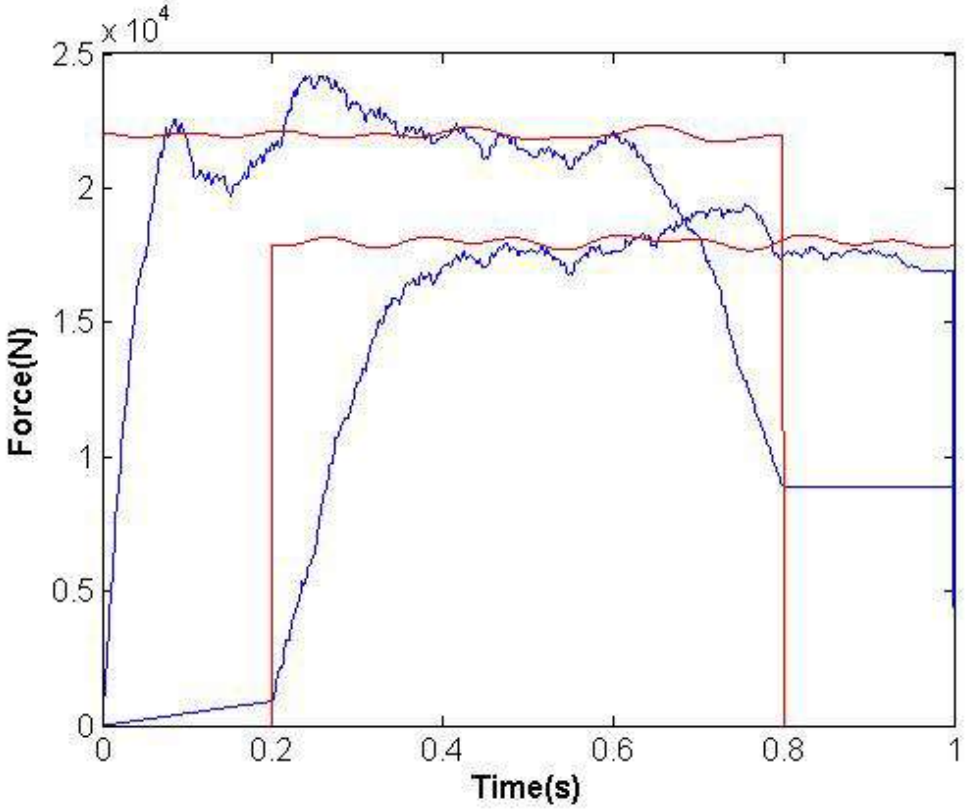

Figure 5.15 – Regularised interaction forces for $\lambda = 1 \times 10^{-18}$ (blue) and corresponding exact applied forces (red), for an empty vehicle travelling at 25m/s on a good profile

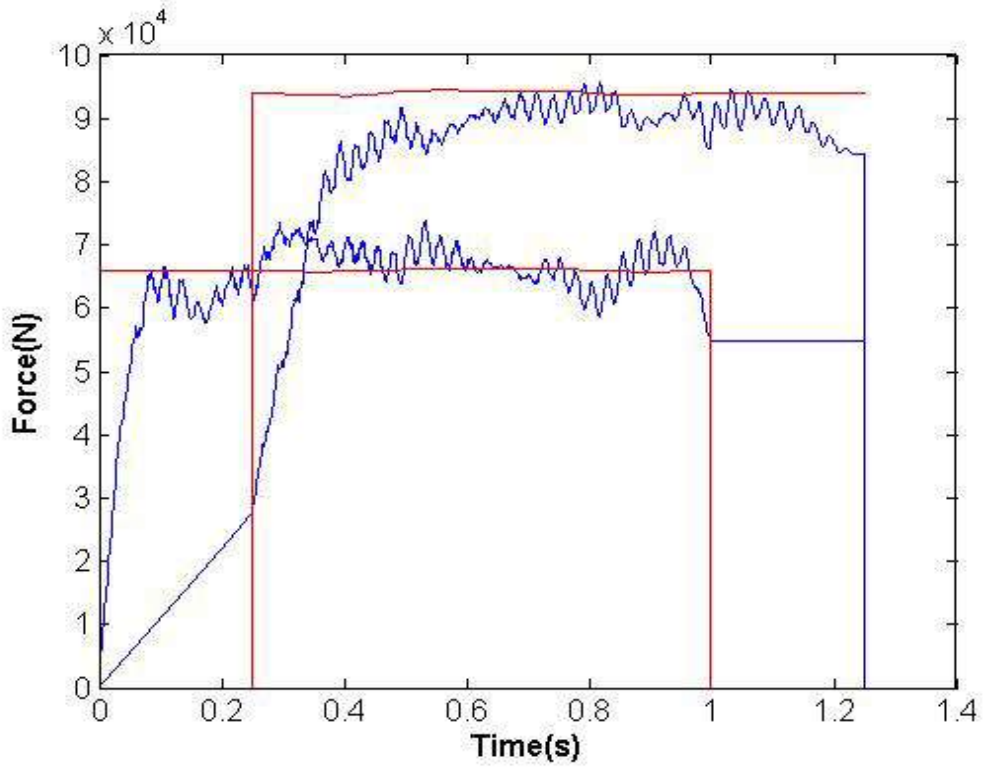

Figure 5.16 - Predicted interaction force (blue) and applied forces (red) versus time for fully laden (14000kg) vehicle travelling at 20m/s on a good road profile, $\lambda = 6 \times 10^{-19}$

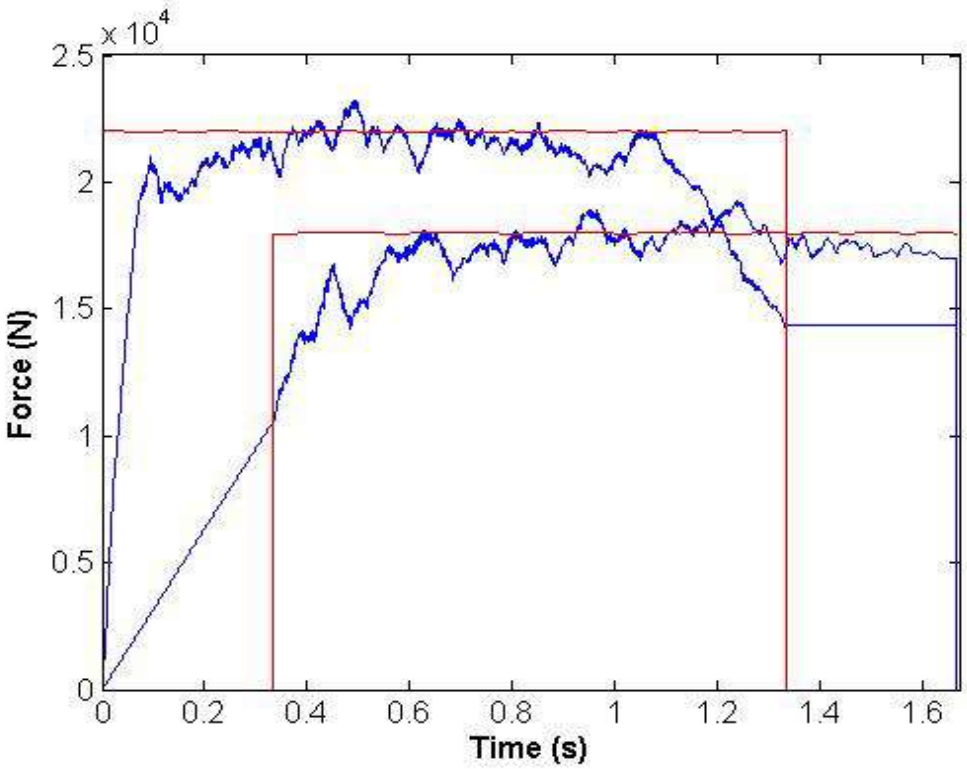

Figure 5.17 – Predicted interaction force (blue) and applied forces (red) versus time for an empty (2000kg) vehicle travelling at 15m/s on a good road profile, $\lambda = 1 \times 10^{-18}$

5.5.3 Results on a rough profile

The same combinations of velocity and loading used in the case of the good profile were used for the rough profile ($a = 128 \times 10^{-6}$ 'poor'). In these poor road profile scenarios, the amplitude of the vehicle dynamics is higher, and the road excites higher vehicle frequencies. For a fully laden vehicle (14000kg) moving at 15m/s the theoretical strain measurements are generated and then contaminated with 3% Gaussian noise see figure 5.18. The optimal regularisation parameter λ was calculated from the L-curve to be approximately 3×10^{-18}, see figure 5.19. Figures 5.20 and 5.21 show the identified interaction forces using the optimal regularisation parameter obtained from the L-curve.

The identified axle force histories compare reasonably well with the applied interaction forces, however there is only one main vehicle dynamic frequency identified in both cases. However on further examination of the L-curve, there is not really a clear point of maximum curvature, but more realistically there is a range of optimal regularisation parameters. What is required is an additional criterion to calculate the optimal regularisation parameter. The criterion proposed herein, is that when the second axle is off the bridge, the corresponding predicted force should be approximately zero, as was the case for the smooth profile and the simulated moving loads.

For the case of the fully laden vehicle travelling at 15 m/s on a poor road profile, the L-curve gave and optimal regularisation parameter of 3×10^{-18}, by moving away from the optimal given by the L-curve, towards a more ill-conditioned solution, the regularisation parameter which minimises the identified forces when an axle is off the bridge can be ascertained. Initially a regularisation parameter of 5×10^{-19} was used as the regularisation parameter in the first order regularisation. Figure 5.22 shows the identified interaction forces versus the theoretically applied axle forces for this regularisation parameter. It can be see from these figures that there is only a slight reduction in the identified forces for this parameter. Moving further away again from the optimal regularisation parameter to an even more ill conditioned solution, where 2×10^{-19} is used as the regularisation parameter in the dynamic programming routine. Figures 5.23 show the identified interaction forces versus the theoretically applied axle forces for this regularisation parameter. It is clear from this figure that the solution for

this parameter is highly ill conditioned and we have moved too far along the L-curve. This process can be repeated by sequentially moving between two successive regularisation parameters. Using this criterion the optimal regularisation parameter was calculated to be approximately 2.6×10^{-19}. Figure 5.24 shows the identified interaction forces using 2.6×10^{-19}as the regularisation parameter in the dynamic programming routine.

For the scenarios of poor road profiles there was generally found to be a large range of values over the region of high curvature of the L-curve. In order to calculate the optimal regularisation parameter for these events, the physical criterion described above is employed. Figures 5.25, 5.26 and 5.27 show typical identified interaction forces using the criterion described above.

It was also found that in the case of resonance, where the frequency of the applied force matches one of the bridges natural frequencies the algorithm still performs equally well. For the scenario of an empty 2 axle vehicle travelling at 20 m/s, it was found that resonance occurs see figure 5.28. The optimal regularisation parameter was calculated as 5e-19 from the L-curve and the aforementioned criteria see figure 5.29, figures 5.30 and 5.31 show the regularised solution for the front and rear axles for the optimal regularisation parameter.

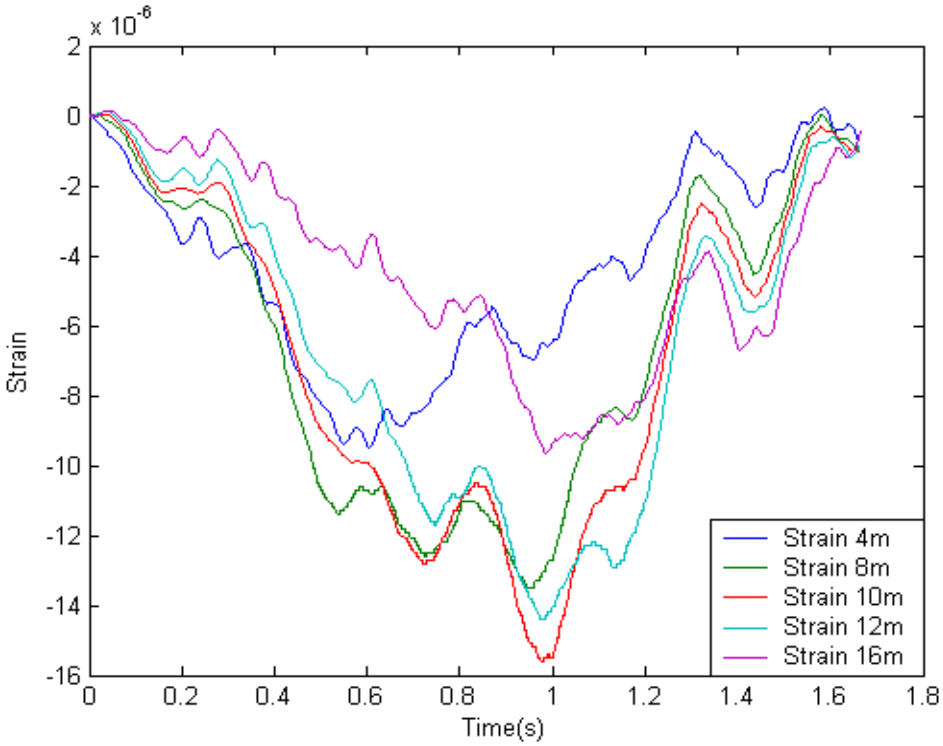

(a) – Theoretical Strains

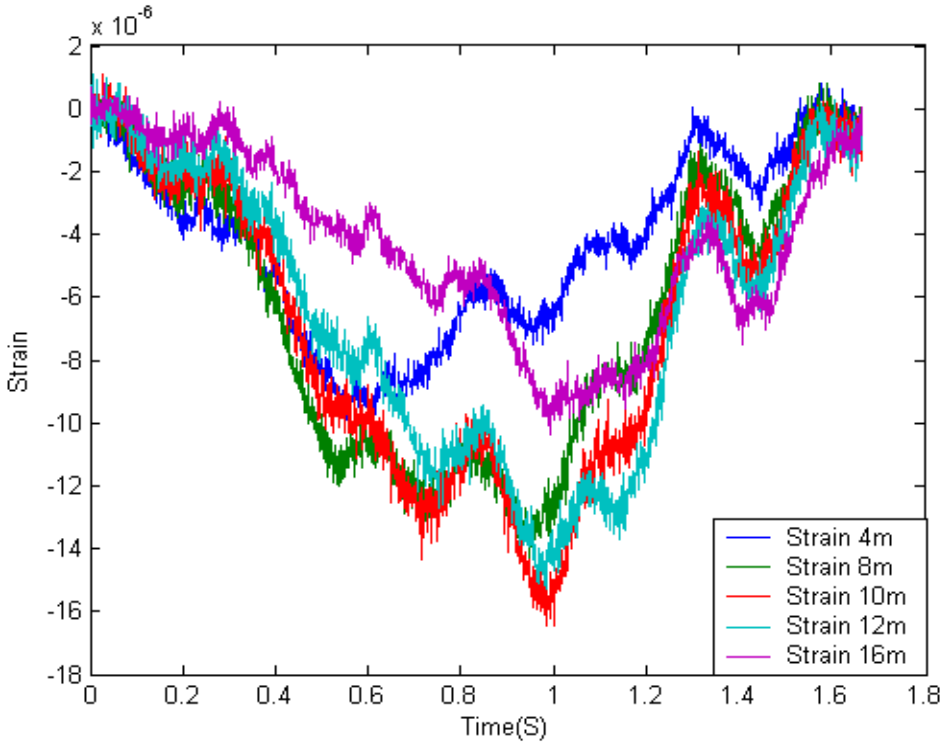

(b) – Noisy Strains

Figure 5.18 – Simulated strain due to an empty vehicle travelling at 15m/s on a poor road profile profile

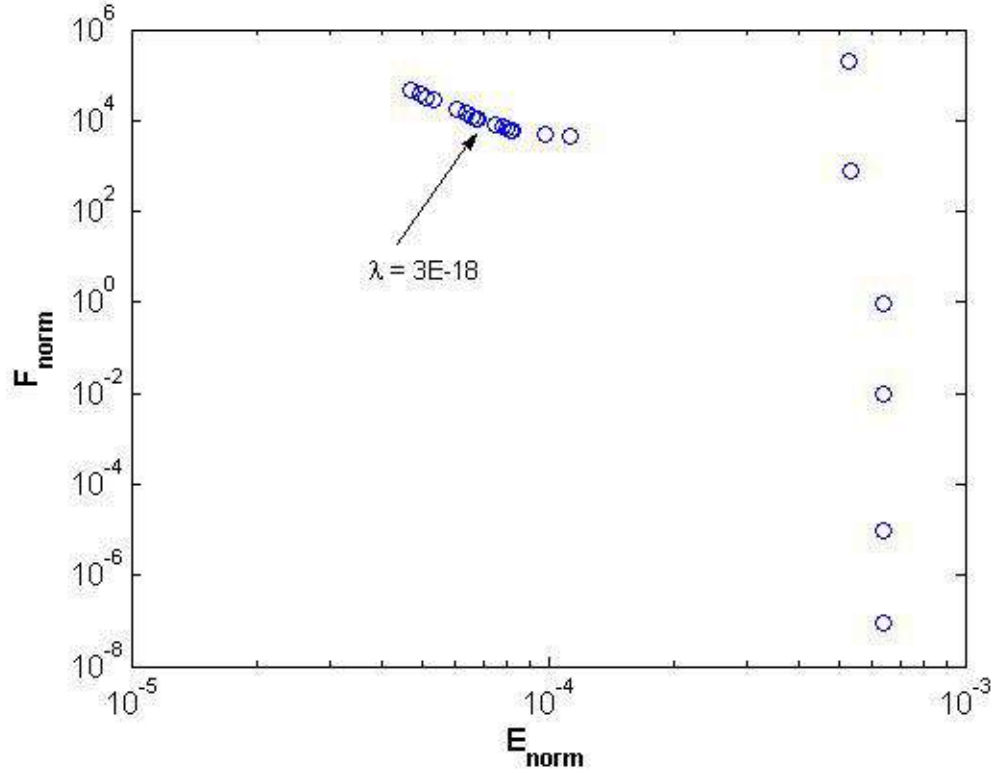

Figure 5.19 – L curve for a fully laden vehicle travelling at 15 m/s on a poor profile

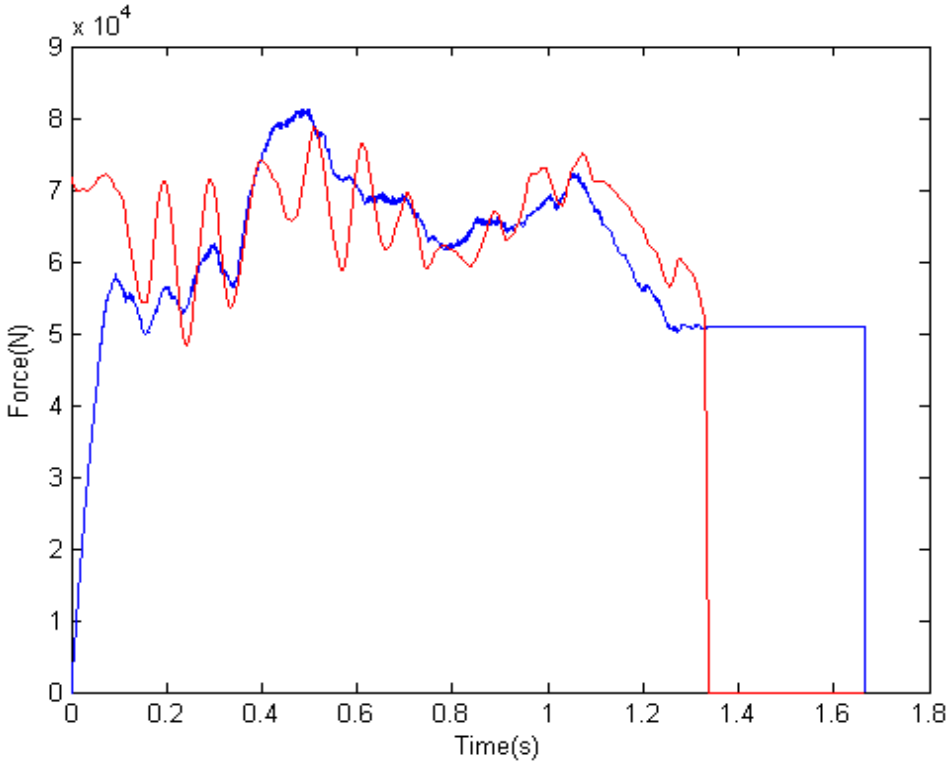

Figure 5.20 - Predicted force (blue) and applied force (red) versus time for fully laden vehicle travelling at 15 m/s on a rough road profile ($\lambda = 3 \times 10^{-18}$), first Axle

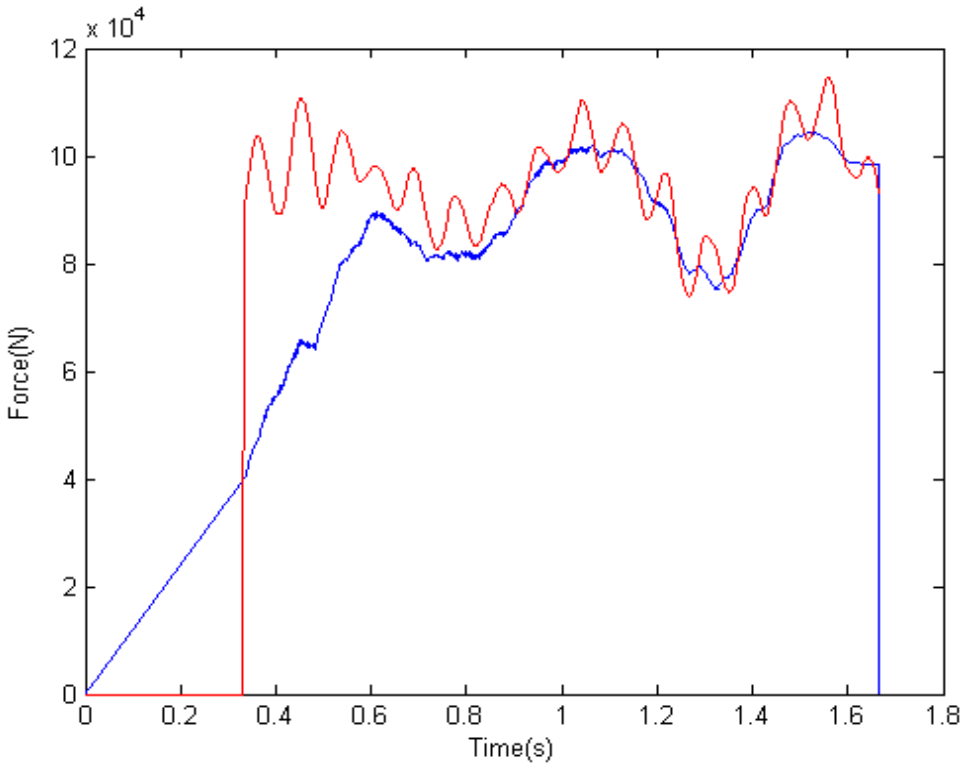

Figure 5.21 - Predicted force (blue) and applied force (red) versus time for fully laden vehicle travelling at 15 m/s on a rough road profile ($\lambda = 3 \times 10^{-18}$), second Axle

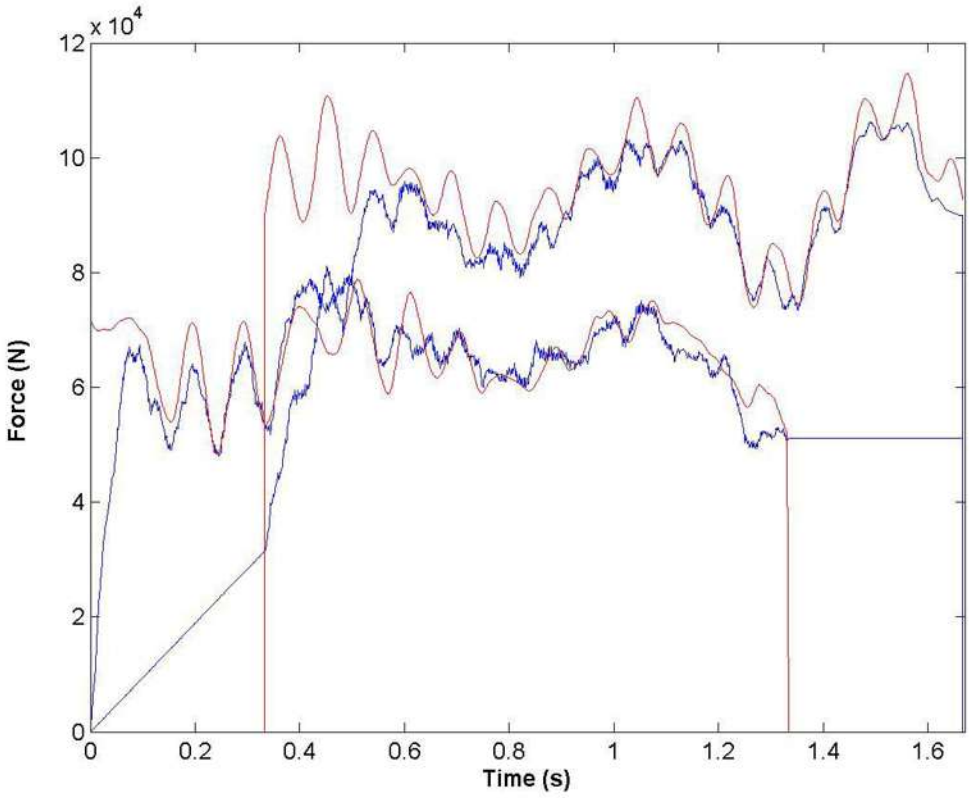

Figure 5.22 - Predicted forces (blue) and applied forces (red) versus time for fully laden vehicle travelling at 15 m/s on a rough road profile ($\lambda = 5 \times 10^{-19}$).

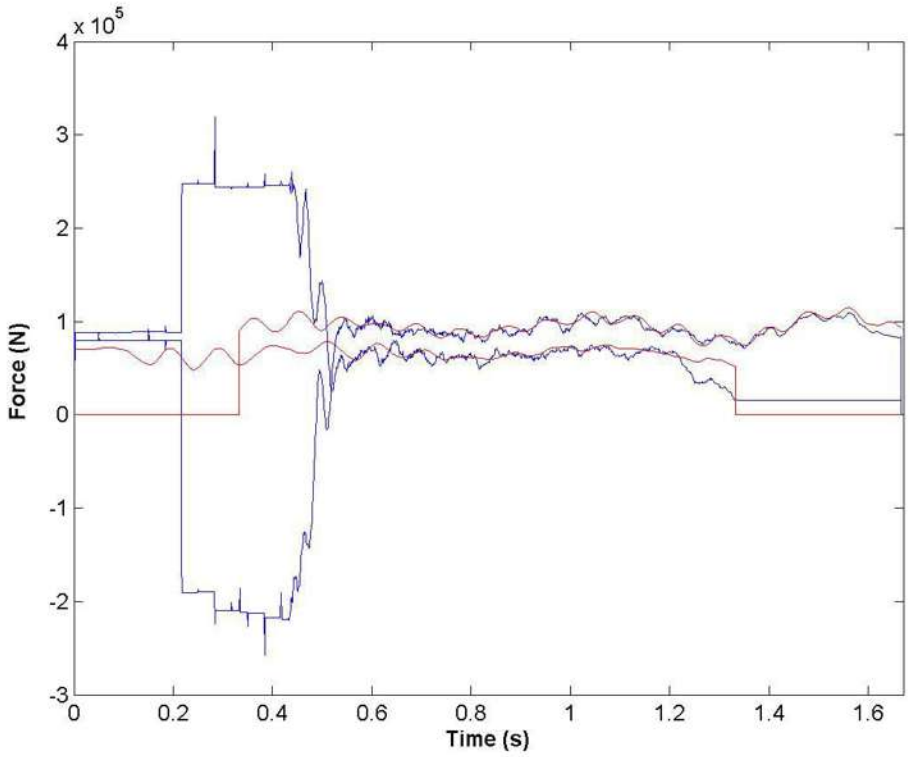

Figure 5.23 - Predicted forces (blue) and applied forces (red) versus time for fully laden vehicle travelling at 15 m/s on a rough road profile ($\lambda = 2 \times 10^{-19}$).

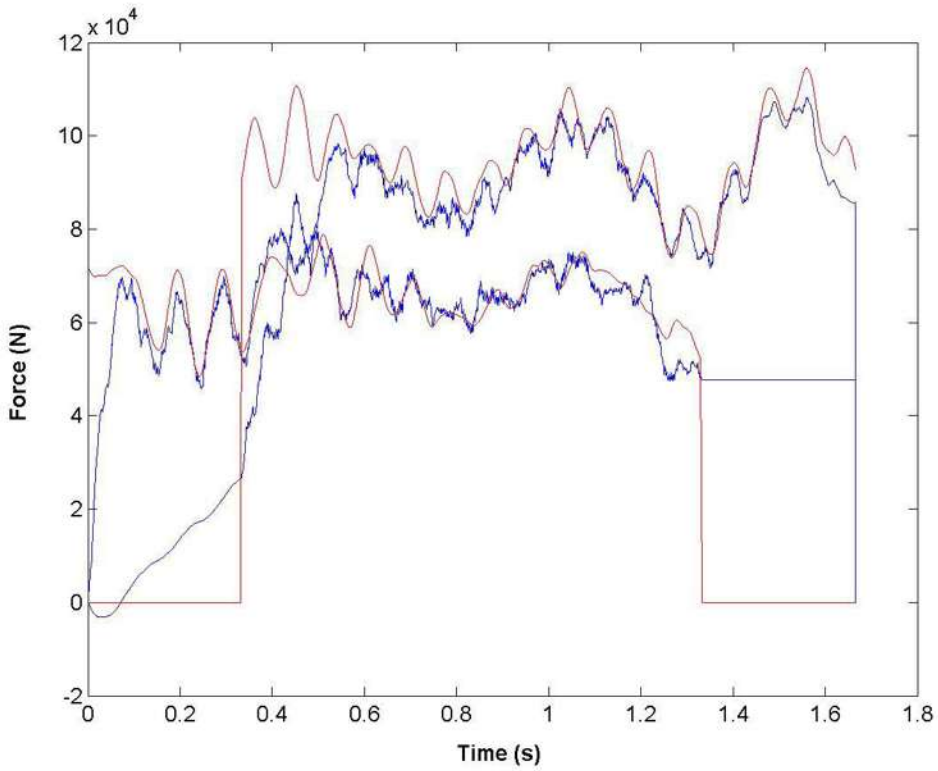

Figure 5.24 - Predicted forces (blue) and applied forces (red) versus time for fully laden vehicle travelling at 15 m/s on a rough road profile ($\lambda = 2.6 \times 10^{-19}$).

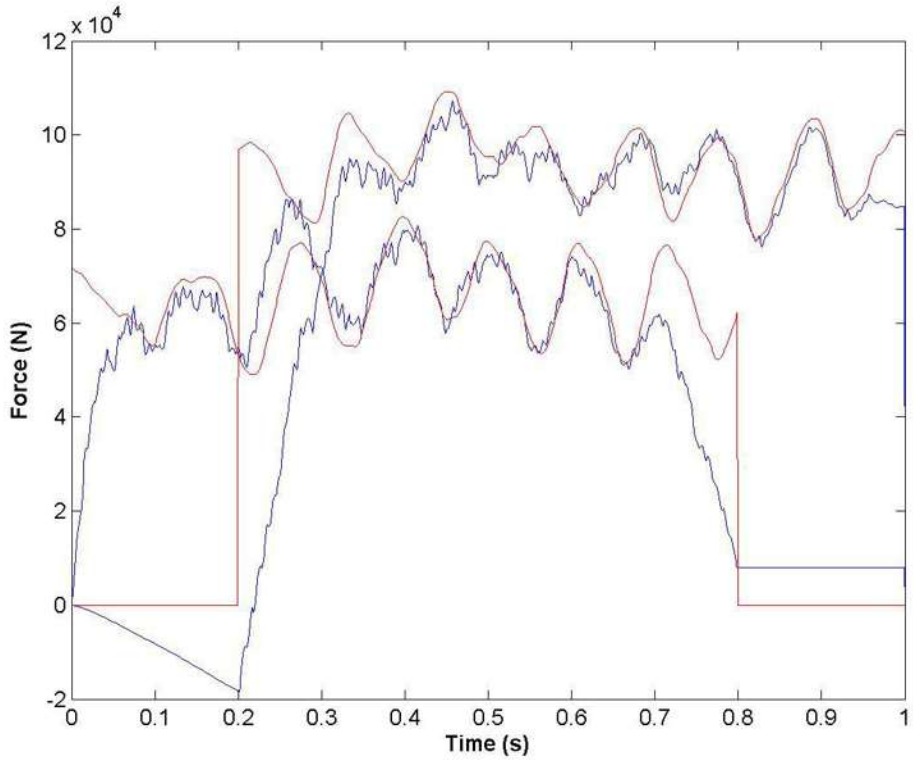

Figure 5.25 - Predicted forces (blue) and applied forces (red) versus time for fully laden vehicle travelling at 25 m/s on a rough road profile ($\lambda = 1.7 \times 10^{-19}$).

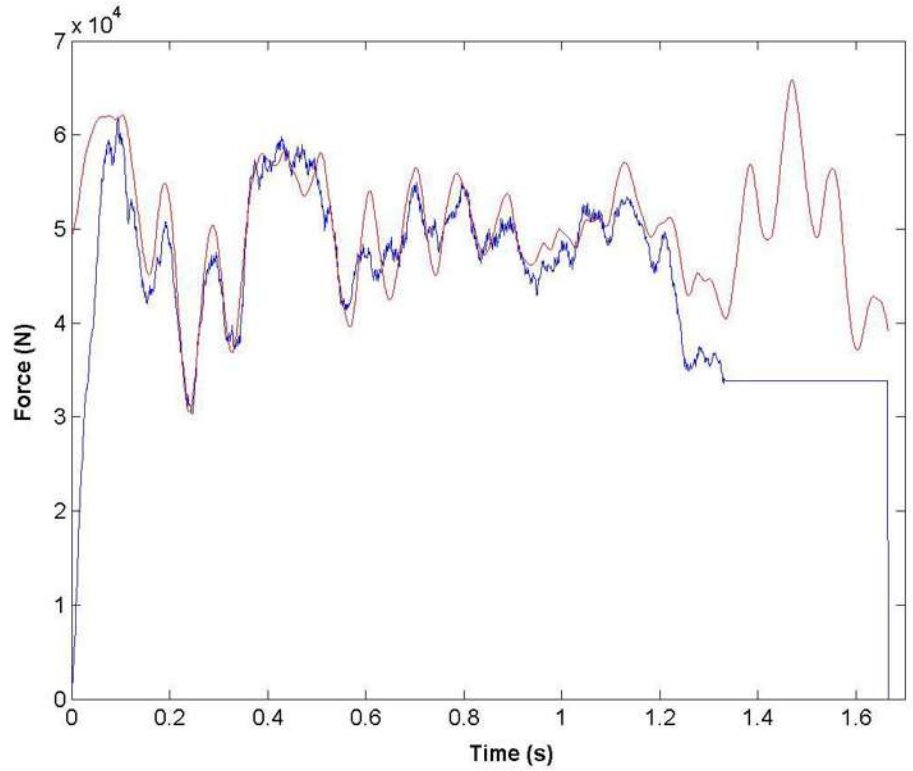

Figure 5.26 - Predicted force (blue) and applied force (red) versus time for half laden vehicle travelling at 15 m/s on a rough road profile ($\lambda = 6 \times 10^{-19}$), first Axle

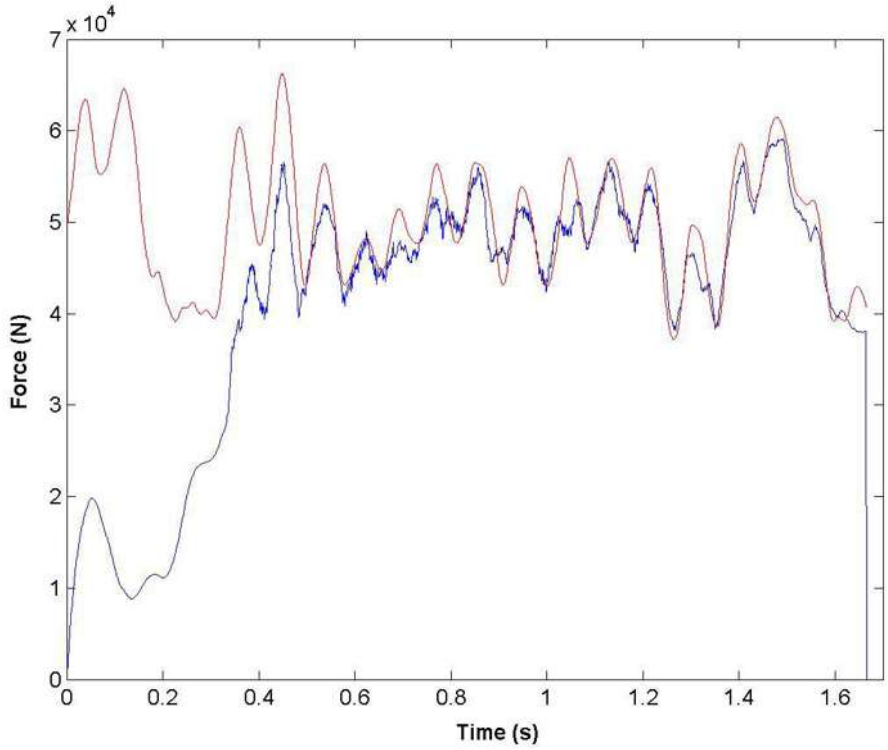

Figure 5.27 - Predicted force (blue) and applied force (red) versus time for half laden vehicle travelling at 15 m/s on a rough road profile ($\lambda = 6 \times 10^{-19}$), second Axle

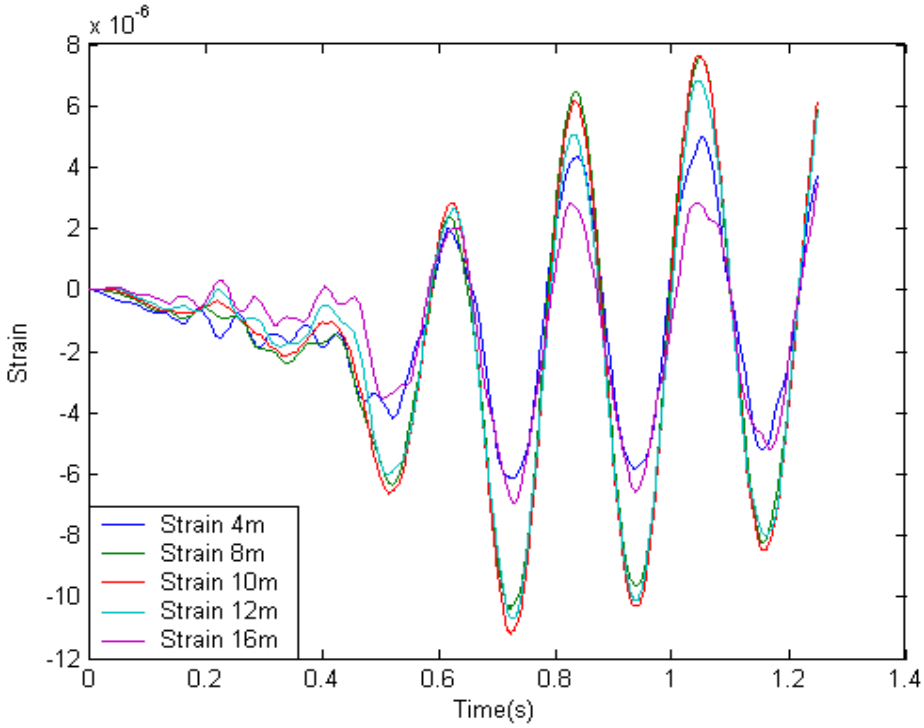

Figure 5.28 – Phenomenon of resonance in simulated strains due to an empty two-axle vehicle travelling at 20 m/s on a rough profile.

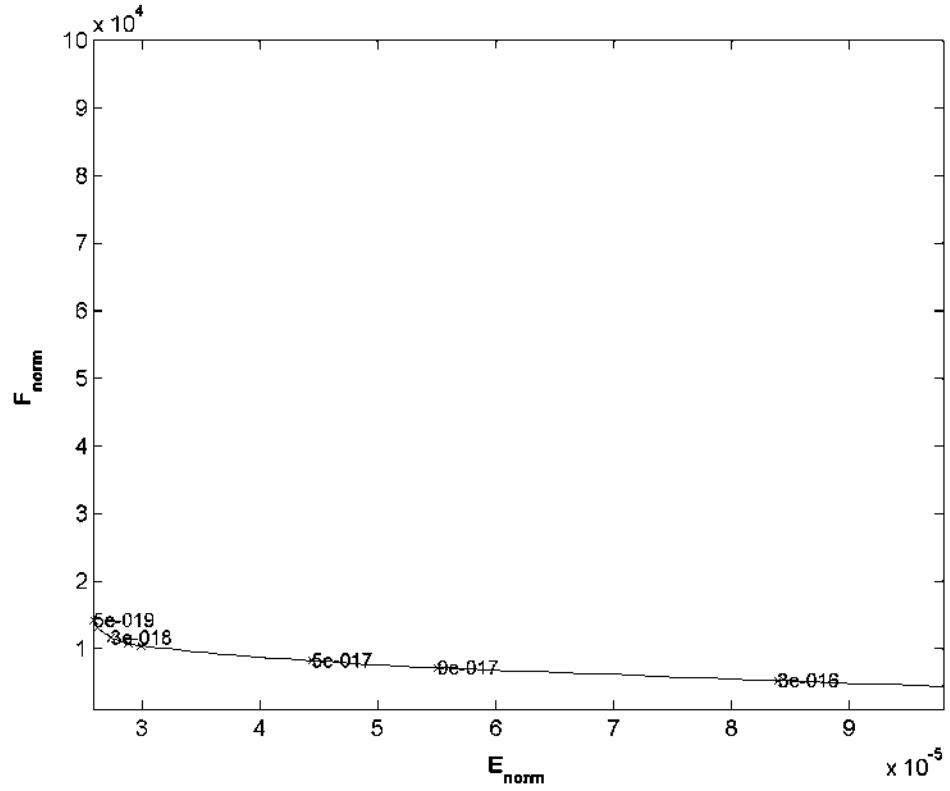

Figure 5.29 – L curve for an empty vehicle travelling at 20 m/s on a rough profile.

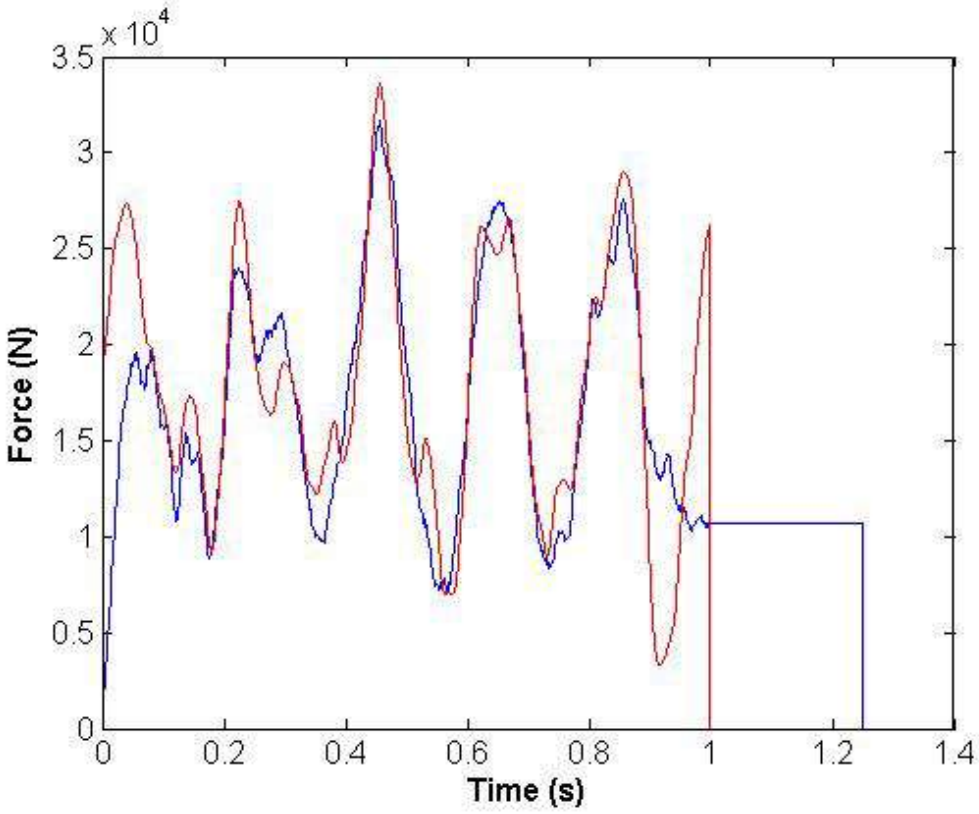

Figure 5.30 - Predicted force and applied force versus time for an empty vehicle travelling at 20 m/s on a rough road profile ($\lambda = 5 \times 10^{-19}$), First Axle

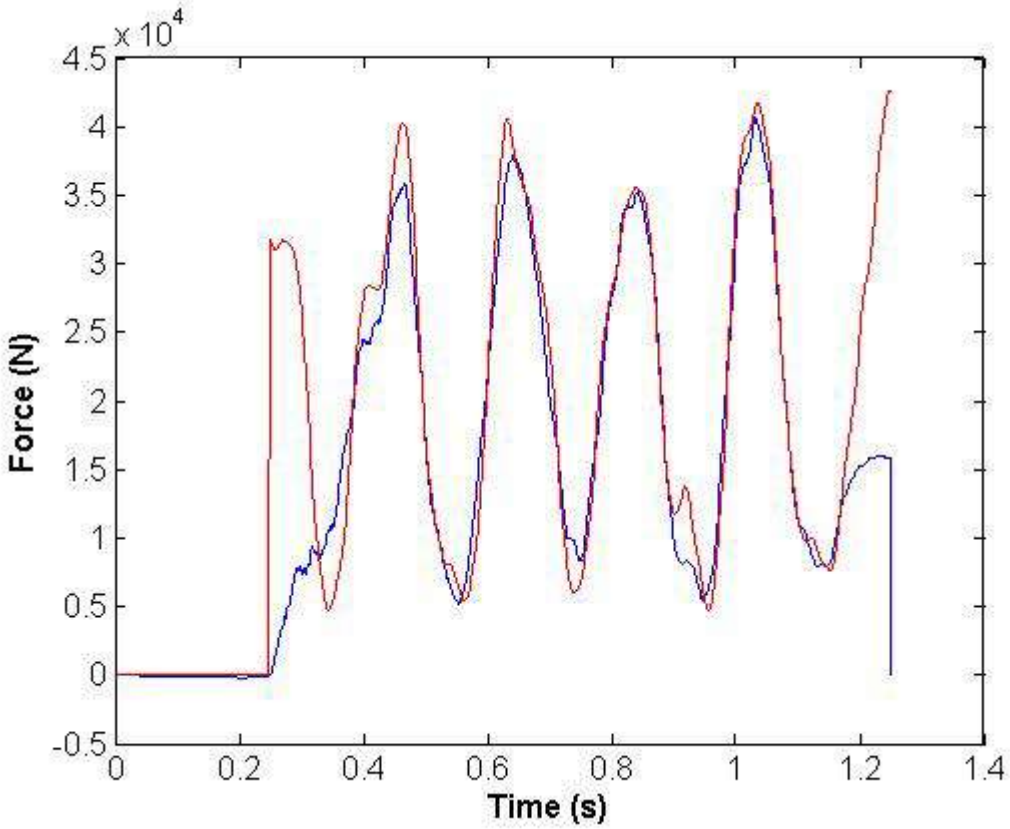

Figure 5.31 - Predicted force and applied force versus time for an empty vehicle travelling at 20 m/s on a rough road profile ($\lambda = 5 \times 10^{-19}$), Second axle

5.6 Comparative study with Moses Algorithm

A comparative study was carried out to assess the accuracy of the static weights inferred from the MFI algorithm with the conventional B-WIM algorithm. The B-WIM algorithm used is the Moses algorithm described in Section 4.3.1. Moses' B-WIM algorithm calculates the static axle weight, so in order to compare this to the MFI algorithm; it was necessary to infer the static axle weights from the regularised time varying force functions. A very simple criterion was employed: 15% of the predicted force from the start and end of the time frame when an axle is on the bridge was removed on the basis that it is likely to be unreliable. The average of the remaining predicted forcing function was calculated and averaged to estimate the static axle weight. The maximum error in gross vehicle weight was 1.9% and 2.7% using Moses' and MFI algorithms respectively. The maximum error in individual axle weights was 8.9% by Moses' compared to 5.5% by the MFI algorithm. The percentage errors in gross vehicle and axle weights for all of the events analyses are given in table 5.1 and represented graphically in figure 5.32. Table 5.1 shows that there is very little difference in the percentage errors between the two algorithms. The reason why Moses' algorithm gives good results is due to the fact that it is reasonably well conditioned for a two-axle system with an axle spacing of 5m. However, if the axle spacing is reduced to 2m and the vehicle is fully loaded, Moses algorithm gives errors of 52% and 29% for the first and second axle respectively, whilst the MFI approach gives errors of only 3% and 5%. This result would indicate that the smaller the axle spacing and the higher the speed, the more significant the improvement in accuracy by MFI theory becomes.

Velocity (m/s)	Load Type	Road Profile	GVW Moses	GVW MFI	Axle 1 Moses	Axle 1 MFI	Axle 2 Moses	Axle 2 MFI
15	Empty	good	1.3	2.0	1.3	2.3	-1.4	1.6
		poor	1.3	2.7	2.4	1.0	0.06	4.9
	Half-full	good	1.4	1.5	1.2	1.3	-1.6	1.8
		poor	1.2	2.4	0.4	3.0	-1.9	2.9
	Full	good	1.3	1.9	1.5	0.07	-1.1	3.2
		poor	0.4	1.2	1.9	-1.2	0.6	2.9
20	Empty	good	0.9	2.2	0.6	0.2	-1.1	3.9
		poor	-2.0	0.2	5.5	1.5	8.2	-0.9
	Half-full	good	0.8	1.9	0.6	1.0	-1.0	2.9
		poor	-0.2	1.9	-1.5	1.1	-1.0	2.7
	Full	good	0.8	2.0	0.5	-0.4	-1.0	3.8
		poor	0.3	2.0	8.9	-2.9	5.6	5.5
25	Empty	good	0.1	1.0	-0.1	1.1	-0.5	1.0
		poor	-0.8	-0.5	-2.2	-3.8	-0.7	3.5
	Half-full	good	-0.04	0.9	-1.06	0.6	-0.9	1.2
		poor	-0.3	0.6	-6	-0.05	-5.7	1.3
	Full	good	-0.3	0.6	0.7	-0.7	1.0	1.5
		poor	-1.9	0.7	-7.6	-1.4	-2.0	2.3

Table 5.1 – Percentage errors in identified weights using the conventional B-WIM algorithm and the MFI approach

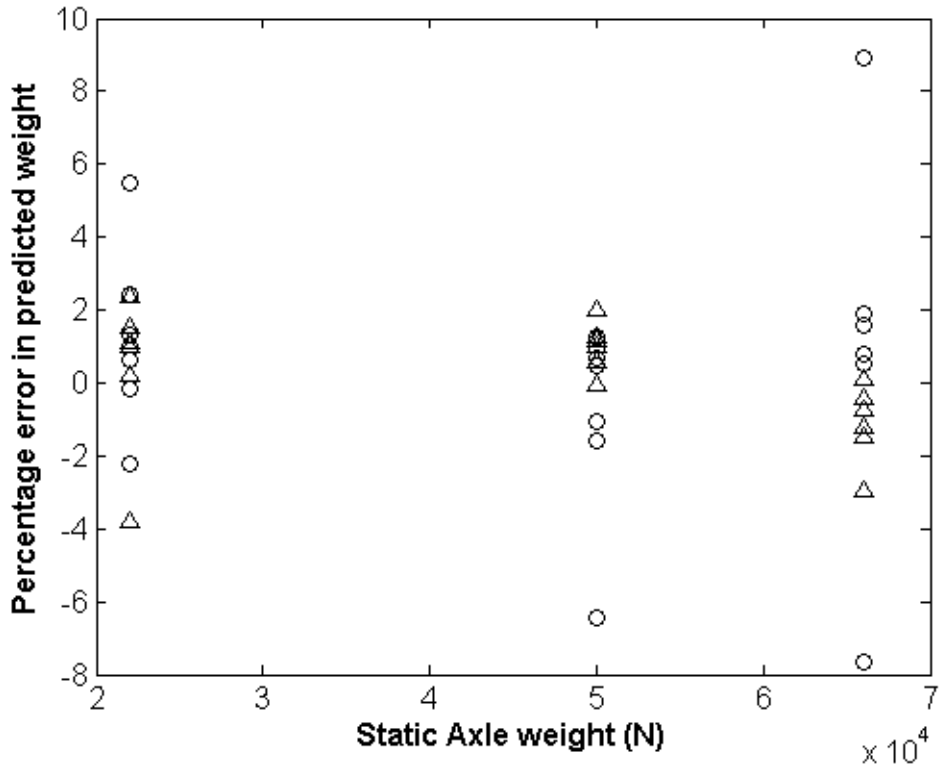

(a) – Front Axle

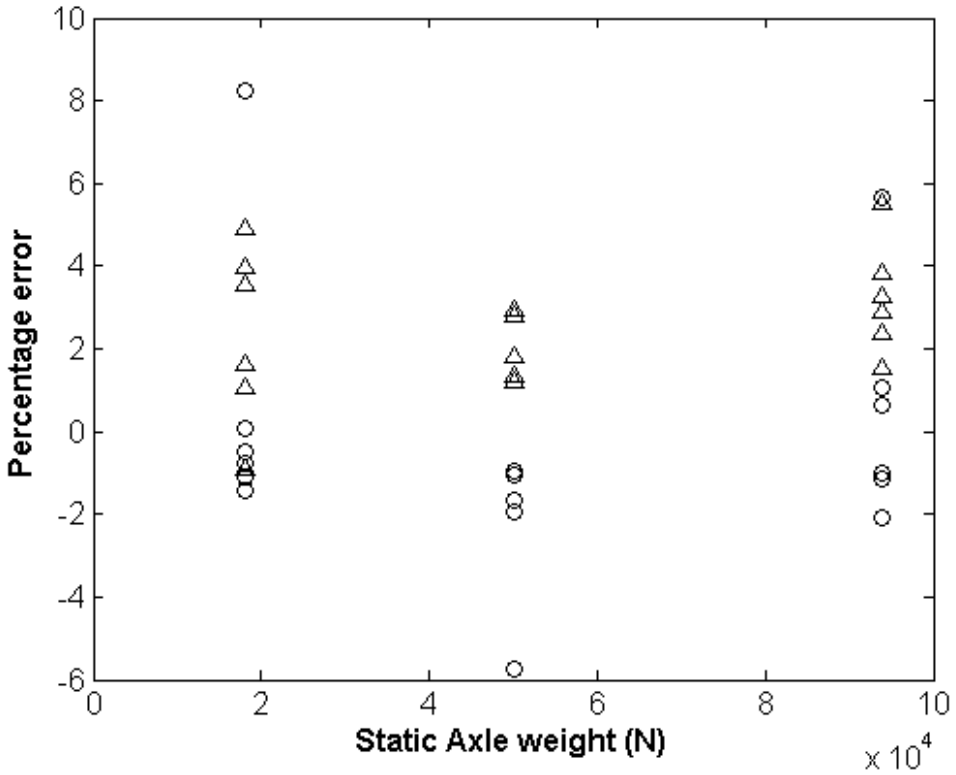

(b) – Rear axle

Figure 5.32 – Percentage error in predicted axle weights versus static axle weight (○ Moses, Δ MFI).

5.7 Conclusions

A moving force identification algorithm based on dynamic programming and first order Tikhonov regularisation has been developed. The algorithm is a direct extension of the theory outlined in Chapter 2. In order to test this algorithm, bridge strains, typically measured by B-WIM systems, are simulated for a number of vehicle crossings. A number of vehicle models have been employed: constant forces, a series of sinusoidal forces and a 4 degree of freedom sprung mass model excited by a road profile.

It has been shown that first order regularisation gives better results than zeroth order. When multiple forces are present on the bridge, it appears to require the number of strain measurement locations be greater than the number of forces. The algorithm has been able to predict multiple forces on the bridge regardless of their magnitude, frequency and phase. The force history has also been accurately predicted for the case of frequency matching between force and bridge.

Finally, the algorithm has been tested using the strains induced in a simply supported beam by a half-car model. The 'measurement' data has been simulated using a Runge-Kutta formulation as described by Frýba while the inverse solution has been obtained using the fist order regularisation of a discretised finite element approach proposed. Results have been obtained for three levels of loading, three speeds and two road conditions, and compared to Moses' static algorithm. The two-axle vehicle has a wide axle spacing and is therefore well conditioned. Hence the overall accuracy is improved only slightly by the new algorithm. This improvement is more significant for the case of rough profile. The difference in accuracy between both algorithms is made clear when using a vehicle of smaller axle spacing, ie, a tandem with a 2 m axle spacing. In this case, the traditional static algorithm proves unable to distinguish forces between very closely spaced axles (error over 50% in individual static axle weight), while the new dynamic algorithm is able to maintain a high level of accuracy. Compared to the traditional static algorithm based on influence lines, the new approach also has the potential to provide amplitudes and frequencies of the applied forces, an additional feature of relevance to the monitoring of traffic loads on bridges.